NOLTR 62-182
DASA-1360

414637

ON THE ORIGIN OF SHOCKWAVES FROM SPHERICAL CONDENSED EXPLOSIONS IN AIR

PART 1
RESULTS OF PHOTOGRAPHIC OBSERVATIONS OF PENTOLITE HEMISPHERES AT AMBIENT CONDITIONS

9 NOVEMBER 1962

NOL

UNITED STATES NAVAL ORDNANCE LABORATORY, WHITE OAK, MARYLAND

NOLTR 62-182

ON THE ORIGIN OF SHOCKWAVES FROM SPHERICAL CONDENSED EXPLOSIONS IN AIR

Part 1
RESULTS OF PHOTOGRAPHIC OBSERVATIONS OF PENTOLITE HEMISPHERES AT AMBIENT CONDITIONS

Prepared by:
L. Rudlin

ABSTRACT: The phenomena occurring during the explosion of pentolite hemispheres are observed using the Beckman-Whitley camera operated at 0.5-μ second intervals. Because of the hemispherical shape, the detonation wave may be followed through the explosive and the resulting airshock followed through the air (for two charge radii). The observations indicate that the airshock formed outside the explosive results from the transmission of the detonation shockfront into the air. The airshock velocity appears to remain constant, at the detonation-velocity value of 7730 m/sec, for several microseconds before decaying in the usual airshock fashion. Comparisons of the hemispherical results are also made with previously unpublished spherical results from Naval Ordnance Laboratory (NOL) experiments and from earlier measurements. There are several discrepancies among these three sets of data revealed by the comparison but not resolved.

PUBLISHED AUGUST 1963

Air-Ground Explosions Division
Explosions Research Department
U. S. NAVAL ORDNANCE LABORATORY
White Oak, Silver Spring, Maryland

NOLTR 62-182 9 November 1962

On the Origin of Shockwaves from Spherical Condensed Explosions in Air

Part 1
Results of Photographic Observations of Pentolite Hemispheres at Ambient Conditions

This report, the first of a proposed series, results from the desire of the author to obtain experimental data on the early behavior of the shockwave from an explosion so that he might employ such data for theoretical calculations. The intended quick look, begun in September 1961, has indicated complexities that now appear to require an extended experimental program. In order to summarize the understanding acquired during this year of experiments this report has been prepared. Since the conclusions and interpretations of this report cannot, as yet, be final, this report should be considered as a progress report, subject to slight or complete modification in later reports.

The material of this report is considered to be of basic importance to explosions research; and the study has been supported by the Defense Atomic Support Agency under Nuclear Weapons Effects Research Subtask 01.003 (Task NOL-181).

R. E. ODENING
Captain, USN
Commander

C. J. ARONSON
By direction

CONTENTS

ILLUSTRATIONS

CONTENTS (Cont'd)

ILLUSTRATIONS

TABLES

ON THE ORIGIN OF SHOCKWAVES FROM SPHERICAL CONDENSED EXPLOSIONS IN AIR

Part 1
RESULTS OF PHOTOGRAPHIC OBSERVATIONS OF PENTOLITE HEMISPHERES AT AMBIENT CONDITIONS

1. INTRODUCTION

1.1 Scope of this Report: Despite the extensive use of spherical condensed explosives for airblast phenomena measurements, little attention has been paid to the detonation behavior of condensed spheres or to the mechanisms by which airshocks are created by spherical detonations. Western literature largely ignores, or idealizes, these phenomena; and the Russian literature available appears to be incomplete (Ref. (1) and (2)).

For clarification of some of the details concerning the early behavior of spherical shockwaves, we have briefly examined and postulated various theoretical models (unpublished work) and found these models required unavailable experimental initial-value data for the theoretical calculations. Further, we have begun to suspect that our understanding of the early explosion phenomena is not adequate for theoretical description. Because of these reasons, and others, we considered the possibilities of performing brief, crude experiments aimed primarily at obtaining a qualitative understanding of airshock phenomena, rather than at obtaining detailed quantitative data from a series of experiments.

There are a large number of experimental difficulties to be overcome in attempting to make measurements at or near the surface of an exploding charge with any physical instruments. We have chosen to dodge these difficulties, at least initially, by using only photographic instrumentation. But photography of full spherical explosions is not very valuable for identifying phenomenological details, since one must observe through a brightly luminous shockfront and cannot observe the transition from detonation shock to airshock.

We have explored, therefore, in this report the use of hemispheres of explosive, which enable us to follow the initiation, detonation, and transmission into air of the spherical wavefront in the explosive. The use of these hemispheres has revealed that the phenomena appear to be far more complex than we had originally suspected and that many additional experiments will be necessary. Further, our photographic data, like all photographic data, require the interjection of the judgment, if not the personality, of the interpreter into whatever conclusions may be drawn from the photographic data. For this reason, we have included, in Section 1.2, an extended outline of our present understanding of the phenomena which has served to guide the interpretation of our photography and have included, in Appendix A, a discussion of the data-processing methods used.

Because we now believe that an extended series of experiments will be necessary to clarify the early airshock phenomena, we plan to report our results in a series of reports, interjecting these experimental reports with theoretical reports as appropriate.

In this first report, we discuss our observations with 2.5-lb. pentolite hemispheres, using the Beckman-Whitley camera at roughly 2×10^6 fps. In addition, we include some previously unpublished data on 1-lb. pentolite spheres taken some years ago at roughly 1×10^6 fps with the Beckman-Whitley camera. These measurements were all made at ambient atmospheric conditions. We hope in a future report to extend our measurements to reduced atmospheric-pressure conditions.

1.2 Background: Detonation in a condensed explosive is indeed a complex problem and is not easily explained theoretically. We do not wish here to discuss the present status of knowledge. For this the reader is referred particularly to References 2, 3, 4, and 5. We believe that it is necessary to outline here some of the theory, in order to clarify our discussion of the origin of the airshock.

1.2.1 Detonation Wave: We define a detonation wave as a region of chemical reaction which moves with a well-defined velocity within an explosive material. The front of the wave is taken to be a shockwave, of thickness on the order of a mean free path. Ahead of the front (moving from the center of the sphere outward) is unreacted explosive. The shock somehow initiates chemical reaction to occur in a finite region of space behind the shockfront called the reaction zone. We consider that the detonation wave proper consists of both the shockfront and the reaction zone. Within the reaction zone occurs non-isentropic flow at extremely high pressures and temperatures for chemical reactions. Behind the detonation wave and extending to the center of the sphere, is a region filled with the products of chemical reaction triggered by the shockfront. This region can be considered to be a rarefaction wave in which the hydrodynamic flow is isentropic. In the ideal plane-wave problem, chemical reaction is completed within the detonation wave, but in the spherical problem burning probably continues into the rarefaction region (cf. Ref. (3)).

The spherical detonation wavefront cannot move at constant velocity (Ref. (3)) but continually approaches the planewave velocity as an upper limit. The hydrodynamic variables, such as pressure, density, local sound speed, and particle velocity are distributed within the reaction zone (i.e., $p = p(r)$, where p is pressure and r is distance) differently for plane and spherical detonations (Ref. (3)).

1.2.2 Reaction Zone: The literature is confusing on the role of the reaction zone for detonation phenomena. Very often the reaction zone is completely ignored or, if mentioned, set equal to zero thickness. Now, this is certainly permissible for those situations and problems in which the reaction zone is of no interest. Certainly this is true for the ideal planewave (time-independent motion) which is most often discussed in the literature. Here, one is most often interested in calculation of heats of

detonations, detonation velocities, and Chapman-Jouguet values of pressure p, density ρ, etc. For such calculations the events within the reaction zone are no concern, since such values are calculable from the hydrodynamics alone and the reaction kinetics within the reaction zone are of little interest. Particularly this is so for gaseous detonations, usually discussed in the literature, for which the reaction-zone thicknesses are much smaller than for condensed explosives.*

For condensed materials, however, we are concerned with reaction-zone thicknesses of the order of several millimeters and characteristic times of the order of a fraction of a microsecond. These are indeed small times and distances but these cannot be ignored when we are concerned with events at the boundary of the charge - a point to which we will return in Section 1.2.3.

Events within the reaction zone are complex, and theoretical descriptions of these events are not abundant. Eyring (Ref. (4)) has suggested that the usual mechanisms of reaction kinetics suffice to explain the processes that occur within the zone. According to Eyring, reaction is triggered by the shockfront (which itself is a pure shockwave) at tiny hot spots on the grains composing the explosive. Opinions differ on the mechanism of triggering. Eyring suggests that the temperature rise produced by the pure shockwave is the source of initiation for burning of the grain, which burning proceeds in the usual chemical sense. The shockwave advances through the explosive material, igniting fresh grains, and sustaining itself by the energy released during the grain burning. The temperature T is a difficult variable to identify in the reaction zone, not only because thermal equilibrium is hardly established within the zone, but also because T is especially sensitive to the equations of state that must be used to describe both the unreacted explosive material and also the reacting grains. Eyring has assumed a T which is an average value of the local temperature of the gases produced by the burning grains and of the temperatures of the grains themselves. Such a definition of temperature leads to values of T as usually considered for detonations - of the order of a few thousands of degrees. On the other hand, Paterson (Ref. (6)), by modifying the Eyring theory slightly to consider that the shockwave primarily heats up the pockets of gas between grains (rather than the grains themselves), has found extremely high values of T - on the order of a million degrees.**

* This occurs because the energy released in the gaseous reaction zone is primarily thermal in origin, whereas for a condensed reaction zone the energy released is primarily elastic in origin. Reference (2) contains an excellent discussion of the solid-state treatment of a condensed explosive. One should recall another important difference between gaseous and condensed explosions: the detonation velocity D is independent of the density ρ_0 for gaseous detonations whereas for condensed explosions $D = D(\rho_0)$.

**Such high temperatures do not seem possible to this author. At the surface of a charge, such temperatures would prevail for at least a finite amount of time and spectra of explosions should be compatible with such temperature sources. The small amount of spectral information available indicates, rather, a cold source - in the order of a few thousands of degrees. It should be pointed out, however, that the mechanisms of light from explosions are by no means clear (Ref. (7)).

Landau and Stanyukovich (quoted in Ref. (2)) have formulated a rather different concept of events in the reaction zone; detonation is considered to result from a deformation of the molecules of the explosive material produced by the shockwave created within the material by the initiator. (We have used the Eyring theory in Reference (3) and have not evaluated the Landau-Stanyukovich theory.)

1.2.3 Events at the Charge Boundary: No matter the mechanism of detonation, at some time the detonation wave arrives at the spherical boundary of the charge. We wish now to consider the phenomena, qualitatively, that may occur at the boundary.

At first, we consider that the outermost grains of molecules constitute a sharp (in the mathematical sense) boundary. When the shockwave, heading the detonation wave within the explosive, encounters air molecules on the other side of the boundary, a shockwave will be immediately (within a time comparable to times between molecular encounters) established in the air surrounding the charge. This necessarily results because infinite accelerations are given to the air molecules first encountered by the shockfront.

As in usual boundary problems, we could require that the pressure and the normal particle velocity be continuous across the sharp boundary. The physical properties of the explosive medium and the outside medium will then determine the physical phenomena that will necessarily be established. For atmospheric air, outside a high-density charge, it is quite clear that a rarefaction wave must occur at the boundary. The pressure of the airshock will necessarily be smaller than that of the detonation shockfront and a rarefaction wave will propagate through the reaction zone, thereby reducing the pressure but increasing the speed of the particles within the zone. If we recall that the reaction zone is a region of non-isentropic flow, we realize that it is quite difficult to derive the necessary boundary equations, relating to pressure and particle velocity across the boundary.*

We remove now our previous restriction that the boundary of the charge is sharp, as indeed it cannot be. When the shockfront, heading the detonation wave, reaches the first air particles to create the airshock, the last grains of the charge surface** will follow the shockfront into the

---

* Stanyukovich (Ref. (1)) and Pack (Ref. (8)) have derived the boundary-transmission formulas for the case of zero-width reaction zone. In this case the rarefaction wave moves into the isentropic region of reaction products which can be readily described mathematically. For a finite-width reaction zone, the rarefaction wave moves through not only a non-isentropic region where burning is taking place, but the rarefaction wave itself may modify the chemical reactions still taking place in the reaction zone (cf., the discussion in Appendix B).

** We refer to particles of radius on the order of 10^{-3} cm, not to pieces of the charge which are occasionally seen flying off the surface of the charge.

air. It seems reasonable to suspect that these grains may continue to burn and to supply energy to the airshock front to support the airshock motion - just as the grain burning within the explosive serves to supply energy to the shockfront to sustain its motion. Such burning would help maintain the speed of the shockfront beyond the charge boundary and delay the decay in shock speed that necessarily occurs when the energy supply to a shockwave is removed.*

What of the gaseous products of reaction behind the detonation wave? Do these gases not contribute energy to the airshock? An answer to these questions on the role of the explosion gases does not appear to be easy and should depend on the precise details of events at the boundary (either sharp or unsharp) and for a finite time interval thereafter. Let us examine the situation qualitatively. It is reasonable to assume (as in Ref. (3)) that there exists some region behind the detonation wave shockfront which is traveling at sonic speed with respect to the shockfront.** If such a sonic zone exists for spherical detonations (directly analogous to the Chapman-Jouguet plane for stationary plane detonations), then it is not possible for energy behind such a sonic zone to reach the shockfront. When the detonation shockfront is transmitted into the air, energy from the reaction-product gases cannot reach the airshock unless

(a) the rarefaction wave (arising from the transmission across the charge boundary) were to increase the particle velocity u^* sufficiently at the previous sonic region (i.e., within the reaction zone the particle velocity u' and sound speed c' are such that $u' + c' > D$, becoming $u^* + c^* = D$ at the sonic zone). If the rarefaction wave increased u' sufficiently (assuming the proper behavior of c'), then the sonic zone could be pushed back into the reaction-products zone, allowing energy to catch up with the shockfront; or

(b) the shock in air were to decay so rapidly that energy could be communicated readily from the reaction-products regime.

It would appear that a detailed study would be necessary for several cases, involving the explosive material, size of the charge (Ref. (3)), conditions of the charge surface (crystal size and chemical condition), and atmosphere-air conditions, before any generalizations could be obtained.

An additional complication must also be considered at the boundary: the second shock. In the original discussion by Wecken and Muecke (Ref. (9)) the second shock was inserted into the mathematical description of the

---

* In Section 3.2.1 we shall present evidence that exterior burning probably does occur to support the airshock speed.

** This assumption is defended in Reference (3) on the basis that a termination to the reaction zone is necessary for stable spherical detonations to be possible, but it is not proved.

characteristics crossing the charge boundary, growing from zero strength. In Reference (3), the second shock has been identified with the infinite derivatives of pressure and the other hydrodynamic variables occurring at the end of the finite-reaction zone (or, what is the same thing, at the beginning of the reaction-products zone). At the present time, the role of the second shock, in influencing the directly transmitted airshock, is not clear. Since, however, the second shock occurs at the sonic zone (the behavior of which will determine whether the gaseous products can contribute energy to the airshock), the second shock may possibly play a role in the early stages of the airshock propagation.

1.2.4 Origin of the Airshock: In the previous sections we have sketched a rather complicated picture of possible events at the birth of the airshock from a spherical, high-density, condensed explosive. (Indeed, the sketch is so complicated at the present time that we are unable to write down the basic equations for the transmission of the shock from the detonation regime to the airshock regime.) Our basic model, however, is that of transmission of a shock across a boundary - from explosive into air. We must point out that other models have been suggested, and below we briefly discuss some of these.

(a) Spherical Shock Tube: In this model the detonation phenomena are completely ignored as such. The detonation serves merely to energize the gases released by the explosive to fill the spherical volume. These gases then expand into the air and at some later time form a shockwave. (This method of creating a shock occurs in linear, compressed-air shock tubes.) Shockwaves can, indeed, be created by spherical shock tubes: the compressed-gas, glass-encased spheres of Boyer (Ref. (10)) create shocks in this manner. But no detonation wave (as it does in an explosive) initially exists in the spherical shock tube model.

Although the author does not know of any reference in the literature specifically suggesting the spherical shock tube mechanism,* the concept is implied in many theoretical treatments, usually for theoretical simplification,** and appears to lurk in the background of many explanations of explosion phenomena.***

* Cook (p. 194-197 and p. 322-326 of Ref. (11)) apparently suggests such a mechanism for explaining his experiments on cylinders.

** For example, the point-source solution of G. I. Taylor and the conservation-of-energy treatment by Kirkwood and Brinkley.

*** For example, the idea that the energy available to the airshock is independent of the ambient conditions outside the charge cannot be based on the concepts of Section 1.2.3.

Stanyukovich (Ref. (1), p. 535-540) discusses the "instantaneous detonation", as opposed to "real detonation", without defining precisely the differences. His instantaneous detonation, "which is equivalent to the dispersion of compressed gas previously at rest and occupying a spherical volume," appears to be what we have termed here the "spherical shock tube", except that the precise mechanism of airshock formation is not stated by Stanyukovich. He states: "The scattering of the products of a real detonation will be similar to the above (a calculation of the instantaneous-detonation maximum distance reached by the gaseous products) only in the initial stage, owing to the fact that the pressure on the front of a real detonation wave is twice as large as the average pressure of the detonation products; the pressure on the front of the shock wave will in this case be higher."

(b) Taylor-wave: Taylor (Ref. (12)) devised a solution to the spherical-detonation problem which has been used by Brode (Ref. (13)) for distributing the hydrodynamic parameters within the detonation wave of TNT spheres. Because the finite width of the reaction zone was ignored, we believe that Taylor's solution is not correct for high-density explosives. (Brode has indicated in Ref. (13) that he encountered trouble in balancing the energy released and the energy available in his Richtmyer-von Neumann machine-code calculations. (Considerable difficulties have also been encountered at the Naval Ordnance Laboratory by Belliveau (Ref. (14)) in the use of the Taylor solution to predict the shocks in air and water from spherical charges.))

(c) The Plasma "Shock": Cook (Ref. (11)) and his colleagues (Ref. (15)) have discussed a rather different mechanism for airshocks.* In this model the initial "shock" from a condensed explosive is really a plasma and perhaps has no shock character. This plasma propagates but a short time in air and is then destroyed by the hot reaction-product gases which soon overtake the plasma. For cylinders, this overtaking occurs, according to Ref. (11), at 2 to 3 cylinder diameters from the end of the charge. The shock that is usually observed, at large distances from the explosion in airblast experiments, is thus formed by the expansion of the reaction-products-gas cloud in a manner perhaps identical to that in a spherical shock tube. We distinguish this model from our model "(a) spherical shock" above because of the plasma "shock" aspect of this model.

*Cook et al have not specifically discussed spherical explosions. Their interpretation of the phenomena observed, however, should not depend particularly on the geometry (although cylinders and spheres differ substantially in the early stages of air shock formation).

2. EXPERIMENTAL DETAILS

2.1 Charges: Pentolite was selected as the explosive material for these experiments for several reasons: the ease with which the material can be detonated, the availability of extensive airblast data, and the immediate availability of pentolite cylinders from which large hemispheres could be machined. In Table I the characteristics of the charges used are given. All hemispheres were detonated by use of Engineer Specials (Hercules) about 3 inches long. The spheres were all detonated by special spherical detonators, manufactured of concentric spheres of silver azide, CH-6, and pressed pentolite, totalling roughly 0.75 inches diameter. These spheres were cast with a cylindrical cavity into which the spherical detonator was later placed; a machined plug was then inserted into the cavity to complete the sphere.

The hemispherical charge is illustrated in Figures 1 and 2. (These photographs are of a wax dummy to model the actual charge.) A lucite disk was glued to the plane side of the hemisphere, primarily to contain any obscuration effects produced by either the detonator or by the charge itself. The thickness of the disk was chosen to be some 2 inches, so that the outermost plane surface of the disk was not spalled or shocked during the time available for the photography. The detonator hole was drilled (9/32 inch diameter) half into lucite and into pentolite, so that the detonator end overran the center of the hemisphere by no more than 1/32 inch. For an actual explosion the charge was supported on lucite sheets with the detonator wires coming out perpendicular to the plane of the plywood table supporting the charge and the lucite sheets.

2.2 Experimental Set-up: All charges were fired inside an NOL bombproof. The Beckman-Whitely Model 189 camera was stationed some 16 feet away from the charge and viewed the explosions either looking directly at the lucite disk of the charge (head-on) or at the spherical surface of the charge (side-on). On the same plywood table holding the charge, a plastic Fresnel lens (some 8.25 inches square) was placed to render parallel the light from an exploding wire source.

High-speed color film was found to be preferable to black and white film for observing and identifying phenomena. The Beckman-Whitley camera, operated at either 1×10^6 or 2×10^6 fps, provided 25 frames on 35 mm film.

Table 1

Characteristics of Pentolite Charges Used

Film No.	Shape	Type	Process	Weight	Diameter	View	Camera	Speed
301	Hemisphere	Cast	Machined*	2.5 lb	5.02 in	Head-on**	Beckman-Whitley	1 x 10^6 fps
325	Hemisphere	Cast	Machined	2.5 lb	5.02 in	Head-on	Beckman-Whitley	2 x 10^6 fps
326	Hemisphere	Cast	Machined	2.5 lb	5.02 in	Side-on***	Beckman-Whitley	2 x 10^6 fps
409	Hemisphere	Cast	Machined	2.5 lb	5.02 in	Side-on	Streak	1.263mm/msec
328	Hemisphere	Pressed	Machined	2.5 lb	5.02 in	Head-on	Beckman-Whitley	2 x 10^6 fps
298	Glob Hemisphere	---	---	7 oz	---	Head-on	Beckman-Whitley	1 x 10^6 fps
339	Hemisphere	Cast	---	2.5 lb	5.02 in	Side-on	Beckman-Whitley	1 x 10^6 fps
118 119 120 121	Sphere	Cast	---	480 g	3.23 in	---	Beckman-Whitley	1 x 10^6 fps

* Machined from cylinder of cast explosive

** Flat side of hemisphere

*** Spherical side of hemisphere

NOLTR 62-182

3. RESULTS

3.1 Detonation Phenomena: Use of the hemisphere charge has permitted us to observe the interior of the spherical detonation. Whether or not we disturb the detonation processes by our configuration from a truly spherical one is simply not answerable. We can hope to deduce an answer from observations on the detonation velocity, which we shall come to shortly.

In Figures 3 and 4 we have printed the frames from films 325 for a cast charge and 328 for a pressed charge (started late in time) to illustrate the motion observable. (The quality of these figures has suffered in the reproduction from the original color film.) In the earliest frames of Figure 3 the asymmetrical detonation of the Engineer Special may be observed. Contrary to previous information, the earliest initiation of the charge occurs off the sides of the detonator rather than off the end. The cardioid-shaped initiation appears to occur on all explosions in a definite pattern with slight variations in the precise shape. In at least one case the initiating shock* appeared to die out in one frame to reappear strongly in the next frame 0.5 μsec later.

3.1.1 Luminous Zone: We assume that the bright zone propagated through the hemisphere is indeed the detonation wave. If we account for the smear naturally produced by the shockfront during the time of the exposure** and the resolution, we obtain a rough value of about 13 - 16 mm for the reaction zone thickness in cast pentolite, a not unreasonable value. After the first μsec or two this luminous zone thickness appears to remain constant throughout the passage of the interior of the charge.

Oddly enough, this luminous zone thickness appears to double (as exact as the measurements can be made) as soon as the shockwave is transmitted into the air and to remain of constant thickness for the distance of observation of about 2 charge radii.

On the other hand our examination of only one pressed pentolite film indicates a different behavior. The luminous zone thickness within the charge is smaller than that for cast pentolite, being roughly 1.1 mm. In the air, the zone width does not immediately double, as with cast pentolite, but grows slowly to about double the interior width at about 2 charge radii. The "gases" may be observed climbing onto this luminous front in air much more violently in the pressed charge pictures than in the cast charge pictures; these gases may obscure the true zone width.

In any event, these crude estimates cannot establish the reality of the luminous zone observed as the detonation wave zone, and we have no need to attempt to do so. What is puzzling is that the luminous zone appears to

---

* That is, the bright cardioid in the vicinity of the detonator.

** The exposure time of the Beckman-Whitley camera at 1 x 10^6 fps is about 0.19 μsec; and at 2 x 10^6 fps, 0.094 μsec.

be so sharply defined at the back end. If the light that we observe as the luminous zone were purely thermal in origin, there should not be so sharp an end and one would expect to see radiation from the reaction gases behind the reaction zone. We do not see such radiation in our pictures.

Occasionally very bright spots are seen superimposed on the luminous zone. We believe that these bright spots result from the passage of the detonation wave through air spaces between the lucite and the explosive. These spots are entirely random in their appearance.

3.1.2 Detonation Velocity: Although it is not completely clear to us that we are indeed observing the detonation wave moving through the explosive material, we have assumed that this is so and attempted to find the detonation-front velocity.

In Figure 5 we have plotted the radius-time data from the three cast pentolite shots which looked head-on into the explosion. (We have included in this figure not only r - t data within the charge but also such data from the airshock outside the charge.) Because of differences in the time of initiation of the detonation in the three shots, the three shots are on slightly different time scales. Since we are primarily concerned with the detonation velocity, we have not attempted to reduce the data to the same time basis. The data shown in Figure 5 have been obtained by finding average diameters of the detonation front; and, thus, some smoothing has been accomplished in obtaining the data of the figure.

For the first μsec or so, after initiation, there is curvature in the r - t data which is not readily apparent from the plot given in Figure 5. Thereafter, the r - t data appear to follow a straight line. We have fitted these data with several n-th degree polynomials (cf., Appendix A) and believe that the best fit to the detonation data is given by a linear fit. Two straight lines are given in the figure. The solid line represents the best linear fit to the data within the charge - giving a detonation velocity of about 7720 m/sec for the cast hemispherical pentolite charges which may be compared to the plane wave value of 7530 m/sec for the cast pentolite given in Reference (16).*

The dashed curve of Figure 5 is our best linear fit to not only the detonation r - t data but also the airshock data for about the first five μsec of time. Our reasons for including the air data will become apparent in Section 3.2.1. The slope of this dashed line to both inside and outside data is about 7450 m/sec - a value within our estimated accuracy of about 5 per cent in detonation velocity.

* Our calculations for TNT in Reference (3) indicated that we should expect the spherical detonation velocity to approach the plane detonation velocity from smaller values. The results for TNT in Reference (3) cannot readily be taken over to predict the behavior of pentolite. These experimental data for pentolite indicate a constant velocity behavior at a time much earlier than obtained in Reference (3) for TNT.

3.2 Airshock Phenomena from Hemispheres: When the detonation wave encounters the edge of the explosive material, the hydrodynamic and chemical events must adjust themselves so as to propagate into the air. Since we have chosen a model for the detonation wave which embodies a pure shockfront heading the detonation wave, we are curious whether such a model is compatible with the experimental observations. (We note that we have not observed any phenomena that are incompatible with this assumption; but we also note that we have no proof of this model.) Our remarks proceed now on the basis that a shockfront, followed by a reaction zone, is transmitted as a shock into the air from the explosive material. Therefore, we look upon this transmission as that of any shock transmission from one medium to another. That the first medium supplies energy, to maintain a constant shock velocity within the medium, to the shock is immaterial. Such an energy supply may serve to perturb the phenomena but does not alter the basic transmission concept that we suggest for the phenomena.

3.2.1 Close-in Airshock Phenomena: Our 0.5 μsec observations indicate that there is a smooth transition of the detonation shock from the explosive into the air. There is no loss of the shockfront and subsequent formation that we can observe with our time resolution. We have estimated that if any such shock formation occurred, along the lines of the spherical shock tube model (Section 1.2.4.(a)), our time resolution was sufficient to observe it.

Indeed, to the contrary, our observations lead us to believe that the "detonation" continues into the air. That is, the r - t data outside the charge can hardly be distinguished from those data within the charge. In order for this to be so, energy must be supplied to the airshock. If this were not so, the airshock would immediately begin to decay, since all shocks must decay in propagation without an energy supply. In Figure 5 we have purposely continued the r - t data beyond the edge of the charge for about 5 μsec to indicate this continuity of the shockfront. The data of Figure 5 suffer from not having a common time base. But for airshock data we may arbitrarily set zero time at the appearance of the shock in air, reducing the radius at zero time to that of the unexploded charge, a_0.

In Figure 6 we have plotted the airshock data for the first 3.5 μsec from four cast pentolite films. One of these films (326) was photographed side-on. We obtained four sets of data from the one explosion by following the airshock transmission along four paths in air from the asymmetrical detonation. One may note from the figure that the data are remarkably reproducible from shot to shot: the data scatter from films 301, 321, and 325 lies within the scatter of data from the four sets of data on the one film 326. We have made linear fits to the first 2.5 μsec and the first 3.5 μsec of growth. The solid curve of Figure 6 is for the former group of data; the dashed curve, for the latter. The slope for the 2.5-μsec line is 7730 m/sec; and for the 3.5-μsec line, 7450 m/sec. We conclude that the airshock travels at constant velocity for about 3 to 4 μsec after leaving the charge -

we cannot precisely determine the time of constant velocity close to the charge within the accuracy of our experiments.*

Unfortunately, our conclusion on the constant airshock velocity must be based solely on our judgment of the data. We could have fitted these close-in data with higher degree (than n = 1) polynomials and found, as would be expected, non-constant shock velocity. We have found for n = 2 and n = 3 polynomials that the initial shock velocity varies from about 8200 - 8800 m/sec depending on the time group of data (2.5 μsec or 3.5 μsec groups). Although we cannot discard these velocities as impossible (cf., Appendix A), we see no reason to require that the shock decay upon transmission into air.

We, instead, can explain the constant airshock velocity with a crude discussion. After the detonation shockfront encounters those last grains of the explosive, it will continue into the air as an airshock. No matter the details of the rarefaction wave that will be set up moving into the center of the explosion, those last grains will continue out into the air and probably continue burning of some kind. The energy released by this burning may catch up and contribute to the airshock front. Let us try to estimate this burning in air.

The time, τ, during which the burning grains of explosive can supply energy to the detonation shockfront has been found by Eyring (Ref. (4)) to be approximately

$$\tau = \frac{a}{D} \frac{\rho^*}{\rho_0} ,$$

for the ideal plane wave. Here

a = reaction-zone length

D = detonation shockfront velocity

ρ^* = density at the end of the reaction zone

ρ_0 = density of the explosive.

We shall assume that a similar relation would describe the time for grain burning in the air behind the air shockfront. If we use subscript 1 for the detonation shock and subscript 2 for the airshock, then the burning time in air is

* We have used a 70-mm streak camera (Table 1) for just the purpose of determining this time more accurately. As of this writing we have not been able to read the streak record happily - identification of the phenomena seen in the Beckman-Whitley pictures and scatter in the streak data have proved troublesome.

$$\tau_2 = \frac{a_2}{a_1}\frac{D_1}{D_2}\frac{\eta_2}{\eta_1}\tau_1 \quad , \text{ where } \eta \text{ is the density ratio;}$$

or if $D_2 = D_1$, as appears to be true from our data of Figure 6, then:

$$\tau_2 = \frac{a_2}{a_1}\frac{\eta_2}{\eta_1}\tau_1 \quad .$$

If we associate the luminous zone of our films with the reaction zone behind either the detonation shock or the airshock, then $a_2/a_1 = 2$. From Appendix B, we will use $\eta_2 = 12$ and $\eta_1 = 7/5$ for rough estimates of the density ratios in air and in the charge. The burning time within the explosive, τ_1, may be estimated from our data of $a_1 \sim 1.5$ mm and $D_1 = 7720$ m/sec to be $\tau_1 \sim 1/4$ μ sec. Hence:

$$\tau_2 \sim \frac{(2)\ (12)}{(7/5)}\ \left(\frac{1}{4}\right) \sim 4\ \mu \text{ sec}$$

a time that appears compatible with our estimates of the time that the airshock velocity remains constant in air.

Our discussion is necessarily crude at the present time; we simply do not know enough about the hydrodynamic phenomena - or the chemical or physical phenomena - at the "boundary" of the charge. For instance, we cannot conclusively rule out contributions to the shockfront from the gaseous products behind the sonic zone as a source of energy supply to the close-in shock. Nor have we considered the role of relaxation phenomena in modifying our understanding of the transmission phenomena. Before we leave this topic, however, we wish to point our that this discussion of the close-in phenomena is not merely one of data fitting or the accuracy of experiments. If such constant velocity behavior of the airshock is physically true, then this is an extremely important bit of information with applications to both further experimental and theoretical research. The difficulty lies in establishing the reality by experimental means.

3.2.2 Airshock Pressures from Cast Hemispheres: From the radius time measurements we can calculate the pressures associated with the airshock leaving the charge. In Figure 7 we have given the calculated peak shock overpressures from our hemispherical explosions viewed both head-on and side-on (cf., Appendix A for computational details). The dashed curve represents the best polynomial fit (in our judgment: n = 2) of all the airshock data, from the charge surface out to the maximum extent of the data at $\sim$ 1.95 charge radii. The solid curves represent what we believe is the truer picture. The upper, constant pressure curve, out to about 1.3 a_0 represents our linear fit, of Figure 6, to the first 2.5 μsec of data. The lower, decaying pressure curve represents our best fit (n = 2) to the r - t data from 3 μsec on. We have used a small dashed curve to connect the two parts of the solid line curve in completely arbitrary fashion, since this part of the curve is unknown to us.

The data of Figure 7 represent only some four explosions: one set of data from three head-on-viewed explosions and four sets of data from one side-on-viewed explosion. Although the reproducibility of the airshock r - t data appears unusually good to us (compared with the much larger scatter found at many charge radii out), the reader should be warned that we have not made a sufficiently large number of explosions measurements to validate either curve of Figure 7.

3.2.3 Effect of the Hemispherical Shape: We have lumped into Figure 7 measurements head-on and side-on (cf., Table 1). Our contention is that we cannot tell r - t data off the plane side from similar data off the hemisphere side.

In Figure 8, we have printed all frames of the Beckman-Whitley film 326 for a cast charge, looking side-on at the explosion, after the detonation wave has reached the outer surface of the charge. Because the initiation is not symmetrical, that part of the charge off the side of the Engineer Special (cf., Fig. 3 or 4) is detonated earliest. In Figure 8, we view the intersection of the spherical detonation front with the spherical charge surface as a plane front moving up the charge surface. The detonated portion of the hemisphere appears bright by comparison with the undetonated portion of the charge surface. This brightness that we view in Figure 8 is probably the airshock and we cannot see into the back of the airshock, as we can in the head-on view. We note from Figure 8 that the inner surface of the lucite nearest the plane surface of the explosive moves off but behind the airshock. Thus the head-on view is not obscured by the presence of the lucite, once the detonation shock has moved into air. Also we may note that the outer surface of the lucite is not reached by the shock in the lucite during the time of observation. In the head-on view the lucite disk edge may be viewed as a circle at late times (cf., the late pictures of film 328 in Fig. 4).

In Figure 9 we have compared data from the head-on films of 325, 321, and 301 with the side-on data from film 326. In order not to obscure the comparison we have shown only the side-on data from 6 μsec on; the side-on data for earlier times has about the same scatter. We conclude from Figure 9 that whatever differences exist between the head-on and the side-on shock configurations, if any, are masked by the natural scatter of the measurements. We have, therefore, lumped side-on and head-on data together into one group.

It is quite likely that the hemispherical shape will introduce perturbations into the flow field so as to disturb a truly spherical configuration. But whether such perturbations ever catch up with the airshock front or modify the observable phenomena at all is not certain. As far as we can detect, over a radius available to us in our experiments of about 2 a_0, the airshock propagation does not appear to be perturbed by the hemispherical configuration that we have used. Our interest in the hemispherical configuration, however, is not mainly in obtaining quantitative airshock data but in being able to see what is going on. We cannot discriminate between a shock-front or gaseous expansion in looking through the airshock at a spherical

surface, either on a hemisphere or a true sphere. The head-on view of the hemisphere enables us to look at the explosion front, and behind it, and to evaluate what is happening.

This point is well illustrated by the events of Figure 10. The 25 frames here are from the Beckman-Whitley camera looking head-on at a hemisphere of Comp C-3. This film was made solely to check out the optical alignment of the set-up used to fire the pentolite hemispheres; we had not planned to utilize the explosion for any other purpose. The charge was, therefore, globed into hemispherical shape by hand and was fired by an Engineer Special. But one can observe, in this head-on view that a luminous zone, which we consider to be a true airshock, leaves one side of the charge whereas only gases (or tiny pieces of explosive) leaves the other side. (This is particularly clear in Frame 15 of the series.) Subsequently, the luminous airshock continues out but does not spread into the region of gases which also spread out. We do not know why the airshock failed to propagate out of one side of the charge; but we doubt that this situation would have been detected in a full spherical situation.

3.2.4 Comparison of Pressed- and Cast-Pentolite Explosions: We have found differences in the airshock behavior from two different forms of the same chemical material. Our present conclusions, however, we caution, are based on only one explosion of the pressed pentolite material. (For certain reasons, too lengthy to dwell upon here, we have not fired additional pressed shots in our limited program.) Our cast shots have proved to be remarkably reproducible and, as of now, we have no reason to doubt the validity of our single pressed charge results.

In Figure 11 we have compared pressed and cast hemisphere radius-time data. The dashed curve is the second-order polynomial fit of Figure 9 for cast data. The symbols represent four sets of readings taken from the single pressed-charge film, and represent the inherent scatter on a given film. To these data points is machine-fitted the solid curve of Figure 11 for a second-order polynomial fit. In our judgment the pressed data are significantly different from the cast data and, thus, possess different pressure-distance curves. In Figure 12 we have made a comparison of pressures using second-order polynomial fits to the cast data of film No. 336 and also to the pressed data of film No. 328. We have ignored here any constant pressure region near the charge surface, as discussed for Figure 7, and used the polynomial fits right up to the surface of the charge.

The puzzling thing about Figure 12 is not that the pressure-distance curves are different - one would expect that from previous detonation-wave results that show substantially different behavior - but that the pressed data are lower in pressure at a given distance. On the basis of grain size alone, one could argue that the smaller grains of a pressed explosive would release energy more readily than those larger grains of a cast explosive; and one should expect a greater pressure from the pressed explosive. Unfortunately, the pressed-charge explosion took place too early for the recording of sufficient detonation-wave motion to establish the detonation velocity.

One easily observable difference between the luminous airshocks of the cast and the pressed explosions is that the reaction-product gases appear to be much more violent, closer to the front of the airshock and to have begun earlier for the pressed charge than for the cast charges. It is not clear to us why this should be.

3.2.5 Effect of Machining upon Airshock: When our first experiments were being planned, it appeared particularly convenient to obtain hemispherical charges by machining this shape from available cylinders of both pressed and cast pentolite. Since past experience had also indicated that machined charges were better charges (in the sense of reproducibility), this convenience seemed desirable also. When, however, we were forced to conclude that burning continued into the air for some time (cf., Fig. 7), we suspected that perhaps this effect was somehow connected with the machining of the charge surfaces. A shot was, therefore, made using a cast pentolite hemisphere (directly cast) of identical size to the previous hemispheres but on which a 2.5-in-diameter surface was machined away. This machined area was placed on the hemispherical side of the charge, to a depth of about 0.003 in, and the explosion was viewed side-on. The film was, unfortunately badly exposed and is not suitable for reproduction here. It appears that the shocks from both the machined and the cast portions move indistinguishably, but explosive gases appearing only from the machined area appear to outrun the shockfront. Another complication was discovered after the shot was made: the neck (of 1-in diameter) through which the explosive was originally poured was in the exact center of the machined area. We detect on the film that the gases from this 1-in surface are particularly violent and farther ahead of the shockfront. Undoubtedly, the machining appears to have caused the gaseous motion, not noticeable elsewhere from the cast surface; but, on the basis of this one confusing test, we cannot be confident of the role that machining does play on the early phenomena.

3.3 Airshock Phenomena from Spheres: Previously unpublished films on spherical explosions were kindly supplied to us by John F. Goertner of the Air-Ground Explosions Division. These films were made, as part of another study on the response of aerodynamic shapes to shockwaves, only to verify the quality of the charge so that pieces of charge would not fly off during the explosion. We present in this section the data from four films of these spherical pentolite explosions made during November 1959.

These charges were cast under carefully controlled conditions. The four charges passed rigid x-ray and visual inspections and were as carefully prepared, armed, and fired as possible. To avoid detonation problems, special spherical detonators were made of concentric spheres of silver azide, CH-6, and pressed pentolite composing a final diameter of about 0.75 in. The charges were cast with a cavity to allow the placing of the detonators at the precise center of the spheres. Cast pentolite plugs were then machined to fill the cavity and complete the spherical-charge shape. The final spherical charge diameter was about 3.23 in and weighed (without the 5-gm detonator) about 480 gm. The approximate weight of the machined plug was 160 gm. At the time of manufacture, these charges were believed to be as good as spherical charges could be made.

In Figures 13 and 14 we have printed the frames from the Beckman-Whitley camera, operated at 10^6 frames per second, on two of these four shots. In Figure 13 the charge is viewed directly; in Figure 14, two views are shown of the same charge, the second view obtained from a mirror at an angle to see another side of the charge. The first frame is a still picture which served as a calibration marker for the film. In both films, but especially in that of Figure 13, we note that radiation appears at the bottom of the charge, prior to detonation of the full sphere. The radiation is sufficiently intense to illuminate the charge which otherwise would not be visible. (The reasons for this radiation escape are not clear.) In the subsequent frames we observe a bright circle, which we believe represents the edge of a luminous shockfront moving toward the camera. These pictures give us as much detail about the early shock growth at sea level as any seen by the author, but still they reveal very little about the phenomena taking place. The most prominent details are the equatorial line and the disk at the bottom of the charges. The line results from the mold (which was necessarily split in two parts for charge removal). The disk results from the early escape of detonator gases, or whatever produced the initial radiation. In the later frames of Figure 14 we can readily note that a sharp bright front leads the gases.

The radius-time data from the four films are remarkably reproducible from one explosion to another. For the first 5 or 6 μsec, three of the four explosions produce identical data. Rather than plot these r - t data, we have given them in Table 2.

In order to make the r - t data from the four films comparable, we have adjusted the data so that at the designated zero time the radius is precisely that of the unexploded charge. This has been done by subtracting from all measured radii the difference between the radius of the airshock in the first frame of appearance and the unexploded radius. Since the time between frames for these films is 1 μsec, the shock could have appeared in the first frame at any time during the 1-μsec interval and the r - t data will necessarily be in error by the amount of the shock motion during this interval between frames.*

We have processed the r - t data for these spheres in the same way as for the hemispheres. In Figure 15 are shown several velocity curves for the sphere data. The short-dashed and the long-dashed curves result from second-degree and third-degree polynomial fits respectively to the r - t data of Table 2. In computing these velocity curves all the r - t data of Table 2 were used as a single group of data. For the solid curve (with data symbols) of Figure 15, we have not used the entire group of data. Instead, we have made straight-line velocity fits for the first 9 μsec of travel. The solid lines do not represent a velocity between the data symbols but merely connect the symbols. According to these calculations, then, for the first 1 μsec of time, the airshock travels at a constant 6720 m/sec; for the first 6 μsec of time, the airshock travels at a constant 6390 m/sec and so on.

* This adjustment of r - t data is necessary for lumping the data from several explosions. We have preferred 0.5-μsec pictures primarily to cut down this unmeasurable initial error in the r - t data adjustment.

Table 2

Spherical Charge Radius-Time Data

Time	Radius (cm) Film 118	Radius (cm) Film 119	Radius (cm) Film 121	Radius (cm) Film 122
0	4.105	4.105	4.105	4.105
1	4.750	4.750	4.858	4.750
2	5.398	5.398	5.398	5.398
3	6.045	6.045	6.261	6.045
4	6.693	6.693	6.693	6.693
5	7.341	7.341	7.450	7.341
6	7.882	7.882	7.988	7.882
7	8.420	8.313	8.636	--
8	8.961	8.961	9.121	9.068
9	9.500	9.500	9.609	9.500
10	10.14	--	9.931	9.931
11	10.69	--	10.47	10.36
12	11.01	--	11.01	10.90
13	11.66	--	11.44	11.34
14	12.09	--	11.88	11.77
15	--	--	--	12.09
16	--	--	--	12.52

Our purpose in making these lumped-data fits has been to determine the time of constant airshock velocity, if any, for these spherical explosions. Because we cannot follow events for the spherical explosions, as we could for the hemispheres, it is more difficult to interpret these spherical data. We are limited to measuring the size of the sphere as a function of time and do not know whether the spherical edge represents a well-formed airshock or gaseous products or whatever (cf., Fig. 10). In any event, we note that whatever we are measuring moves slower for the spheres than for the hemispheres. For the hemispheres (Section 3.2.1) we have found a constant velocity of 7730 m/sec for the first 2.5 μsec, and velocities up to about 8200 m/sec for polynomial fits of $n > 1$. The spherical velocities, from the comparable numerical treatments, are much smaller. In our judgment, the spheres exhibit a constant-velocity behavior but it is not as clearly defined as for the hemispheres. From Figure 15 data for the lumped fits we would estimate that the velocity is constant at about 6500 m/sec for about 5 μsec for the spherical explosions - as compared to the constant velocity of 7730 m/sec for about 2.5 μsec for the hemispherical explosions.

3.4 Airshock Pressures from Cast-Pentolite Explosions: In Figure 16, we have summarized the pressure-distance curves from three sources: NOL hemispheres, NOL spheres, and BRL spherical measurements by Sultanoff in Reference (17). The solid curve representing the hemispherical data has been taken directly from Figure 6; the data symbols give the pressures derived from the films at 0.5-μsec intervals. The short-dashed curve connects the derived pressures from films taken at 1-μsec intervals and represents, as for the solid curve, our interpretation of the phenomena occurring in the films. We have superimposed the BRL data for comparison. Out to about 1.5 a_0 these three sets of data appear to be rather different. Since the NOL sphere and hemisphere data were processed identically, the differences between these two curves appears to be real. The BRL data, according to Sultanoff, were obtained from second- and third-degree polynomials and may differ from our results because of the numerical treatment.* It would appear from Figure 16 that by about 2 a_0 the pressure-distance curves are indistinguishable.

It is of interest to ask: how do the NOL and the BRL data compare when treated by the same numerical procedures? In Figure 17 we have drawn the BRL curve (over a larger distance) obtained from $n = 2$ and $n = 3$ fits with NOL curves resulting from $n = 2$ fits to our hemisphere and sphere data. In this comparison, the BRL curve is at most about 10 per cent greater than the NOL sphere curve but some 50 per cent greater at 1 a_0. At about 2 a_0 the sphere data from both sources appear to be in agreement. The hemisphere curve appears to start deviating at large R/a_0 in Figure 17, but this probably results from the numerical fitting. The fitting of Figure 16 to the data beyond the constant-pressure region does not indicate any deviating behavior.

* We have not been able to evaluate the BRL r - t data for the early constant-pressure region because no r - t data have been given in Reference (17). We have, however, used recent equation-of-state data to convert the velocities of Reference (17) to pressures. The differences from the Kirkwood-Brinkley-Richardson pressure values of Reference (17) are negligible and we have given here the original pressures as given in Reference (17).

4. CONCLUSIONS

4.1 Detonation Effects:

(a) Initiation is easily established in the cast pentolite hemispheres and the detonation velocity, within a microsecond or so, appears to become and to remain constant at about 7720 m/sec, very closely the ideal plane-wave value for cast pentolite.

(b) The luminous zone observable within the explosive material seems to represent the reaction zone behind the detonation shockfront. If so interpreted, the reaction zone width in cast pentolite is about 1.3-1.6 mm and in pressed pentolite about 1.1 mm.

4.2 Airshock Effects:

(a) The detonation shockfront appears to be transmitted across the explosive-air interface to create the shock in the ambient air. The airshock velocity appears to remain at the detonation front value for several microseconds after passage into the air.

(b) There is no evidence of any particles running ahead of the airshock front. No gases or pieces of the explosives which should be observable, outrun the airshock, at least out to a distance of about 2 a_0. If electrons or ions outrun the airshock front, their presence was not found in the films.

(c) The luminous region observed in the air appears to be precisely twice the width of the luminous region observed in the explosive. Turbulent gases may be observed riding into the luminous zone but never outrunning the leading edge. The turbulence for pressed pentolite is much greater than for cast pentolite.

(d) The radius-time growth of the airshock from hemispherical explosions appears to be independent of the side of the hemisphere. That is, radius-time data from the curved surface (side-on view) are not distinguishable from the data from the plane surface (head-on view).

(e) The airshock pressure, deduced from the velocity measurements of the airshock from cast pentolite hemispheres, is constant for about 1.3 a_0 at about 9700 psi, after which the pressure decays with distance from the explosion.

(f) Limited data indicate that pressed-pentolite airshock pressures are lower than those from cast-pentolite airshocks. The process of machining used to make the hemispheres of these experiments may have affected the airshock behavior as compared to the airshock from ordinary cast charges. But the effect is not yet clearly important.

(g) Airshock measurements from true spherical explosions of cast pentolite charges indicate close-in airshock velocity and pressure are considerably lower than those for the hemispheres of this study and for the spherical explosions of Reference (17). By about 2 a_0 the pressures for all three sets of explosions are about the same.

4.3 Concluding Remarks: During the course of the experiments described in this report our original ground rules necessarily became more and more changed. Originally we had hoped to take a quick and dirty look at the transmission of a detonation shockfront into air to see if, indeed, such transmission did occur or whether the airshock was formed by some other process. Unhappily, we soon realized that no such quick look could be made, since the phenomena we wished to observe were inextricably related to our choice of many variables - the size of charge, the condition of the surface, the density of the charge, the mechanical form of the explosive - and we could not be sure of the importance of these, and other, variables. Even more unhappily, we realized that the list of experiments, and repetitions that needed to be done was growing beyond bounds. Further, at the same time that these experiments were being performed close-in (less than 2 a_0) to the explosion, another group of experiments* were revealing phenomena from about 20 a_0 on that, in several aspects, appear to complicate our understanding of the airshock from spherical explosions. This report, therefore, cannot, and should not, be regarded as more than a tentative examination of the early airshock phenomena from pentolite hemispheres at ambient air conditions. Our conclusions have necessarily been based on our understanding and interpretation of the phenomena as we think they occur in our photographic films. Other interpretations are not only possible but perhaps desirable to explain future experiments.

With these cautions understood, the author believes that these experiments reveal that, for the conditions of these experiments, the airshock from a spherical explosion is created by the transmission of the detonation shockfront into the air; that this shock travels with constant velocity (and pressure) for some distance from the charge, and then begins to decay in velocity and pressure; that the hydrodynamic phenomena, at least within 2 a_0 appear to be not unreasonable or unusual. As of now, we cannot yet write the transmission equations across the explosive-air interface because of lack of knowledge of the precise phenomena needed to write down the correct equations (cf., Appendix B). Although our interpretation of the airshock motion being constant may be novel, there is nothing incompatible with the usual type of hydrodynamic picture. We realize, however, that we are omitting in this report any attention to the gas products behind the airshock and the role that these gases may play in the airshock growth. That the gases have an important role appears clear to us from the experiments we plan to discuss in Part 2.

* These experiments will be reported in Part 2 of this series of reports at an early date.

Our present conclusions differ from those of Cook and his colleagues (Ref. (11), (15)) who find it necessary to describe a plasma preceding what they interpret as a shockfront in air. We do not understand the statement of Reference (15) that "the observed velocities (of Ref. (15)) would imply a breakdown of the hydrodynamic theory of transmission of shockwaves." In our opinion, the hydrodynamic data of Reference (15) may be interpreted as we have our data here. We have not examined the data of Reference (15) (and the references therein) in detail. We do not believe, however, that our results here require the interpretations of Cook and his colleagues.

In future reports we hope to clarify the airshock behavior from spherical explosions of chemicals other than pentolite, in atmospheres other than ambient air, to distances greater than 2 a_0, and with instrumentation other than cameras.

The author is indebted to Mr. Peter Hanlon and his co-workers of the Air-Ground Explosions Division for much of the film analysis; to Mr. Carl Brown, of the Chemical Engineering Division, for his preparation of the charges; and especially to Mr. Howard Katz and his co-workers, of the Explosion Dynamics Division, for performing the experiments.

5. REFERENCES

(1) Stanyukovich, K. P., Unsteady Motion of Continuous Media, Pergamon Press, New York, 1960

(2) Zeldovich, Ia. B. and Kompaneets, A. S., Theory of Detonation, Academic Press, New York, 1960

(3) Rudlin, L., "An Approximate Solution of the Flow Within the Reaction Zone Behind a Spherical Detonation Wave in TNT," U. S. Naval Ordnance Laboratory, NAVWEPS 7364, 3 Apr 61

(4) Eyring, H., Powell, R. E., Duffy, G. H., and Parlin, R. B., "The Stability of Detonation," Chem Rev 45, 69, 1945

(5) Evans, Marjorie W. and Ablow, C. M., "Theories of Detonation," Chem Rev 61, 129, 1961

(6) Paterson, S., "The Structure of the Reaction Zone in a Detonating Explosive," Fifth Symposium (International) on Combustion, Reinhold, New York, 1955

(7) Ericcson, Ulf, "On Luminous Shock Waves," Defense Research Institute (Stockholm) 30 Jun 59, Unclassified (Also: JPRS No. 8812, 1 Sep 61)

(8) Pack, D. C., "The Reflection and Transmission of Shock Waves, I: The Reflection of a Detonation Wave at a Boundary," Phil Mag 2, 182, 1957

(9) Wecken, F. and Muecke, L., "Detonation d'une Charge Spherique," Parts I and II, Laboratoire de Recherches Techniques de Saint Louis Reports 8/50 and 1/53, 1950 and 1953 respectively

(10) Boyer, D. W., "Spherical Explosions and Implosions," Institute of Aerophysics (University of Toronto) UTIA Report 58, Nov 59

(11) Cook, M. A., The Science of High Explosives, Reinhold, New York, 1958

(12) Taylor, G. I., "The Dynamics of the Combustion Products Behind Plane and Spherical Detonation Fronts in Explosives," Proc Roy Soc (London) 200, 235, 1950

(13) Brode, H. L., "Blast Wave from a Spherical Charge," Phys of Fluids 2, 217, 1959

(14) Belliveau, L. J., "Presentation at the Tri-Partite Conference," 11 Sep 62, held at the U. S. Naval Ordnance Laboratory

(15) Bauer, A., Cook, M. A., and Rogers, L. A., "Ionization Waves from Free Surfaces of Detonating Explosives," Institute of Metals and Explosives Research, University of Utah, AFOSR-1335, 7 Sep 61

(16) "Explosion Effects Data Sheets," U. S. Naval Ordnance Laboratory, NAVORD Report 2986, 14 Jun 55 (Revised)

(17) Sultanoff, Morton and McVey, Gertrude, "Shock Pressure at and Close to the Surface of Spherical Pentolite Charges Inferred from Optical Measurements," Ballistic Research Laboratories Report No. 917, Aug 54

(18) Lehto, D. L. and Belliveau, L. J., "The Treatment of Airblast Radius-Time and Pressure-Distance Data by the Use of Polynomial Approximations with Applications to Pentolite Data," U. S. Naval Ordnance Laboratory, NOLTR 62-85, 15 Mar 62

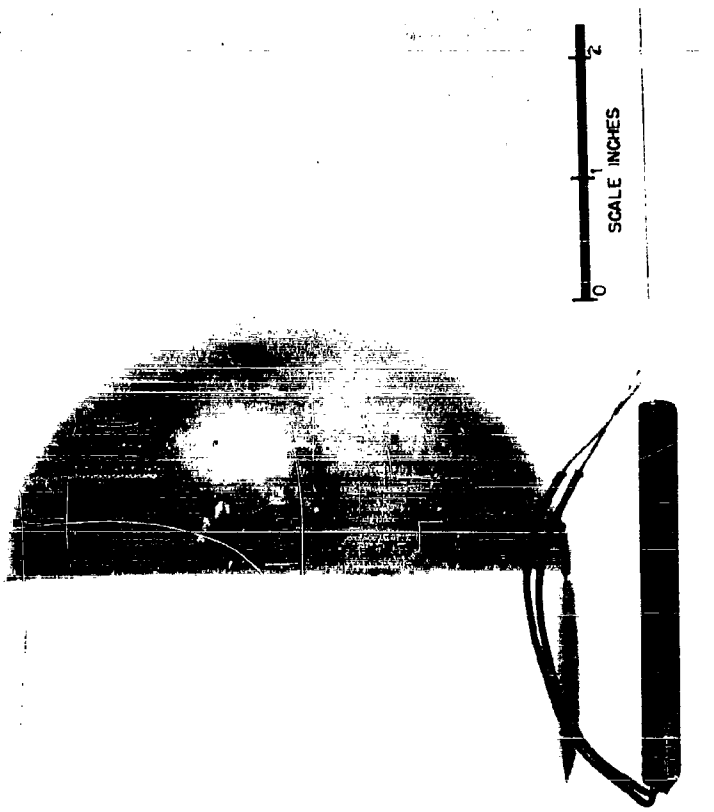

FIG. 1 HEMISPHERE CONFIGURATION: SIDE-ON VIEW (WAX CHARGE)

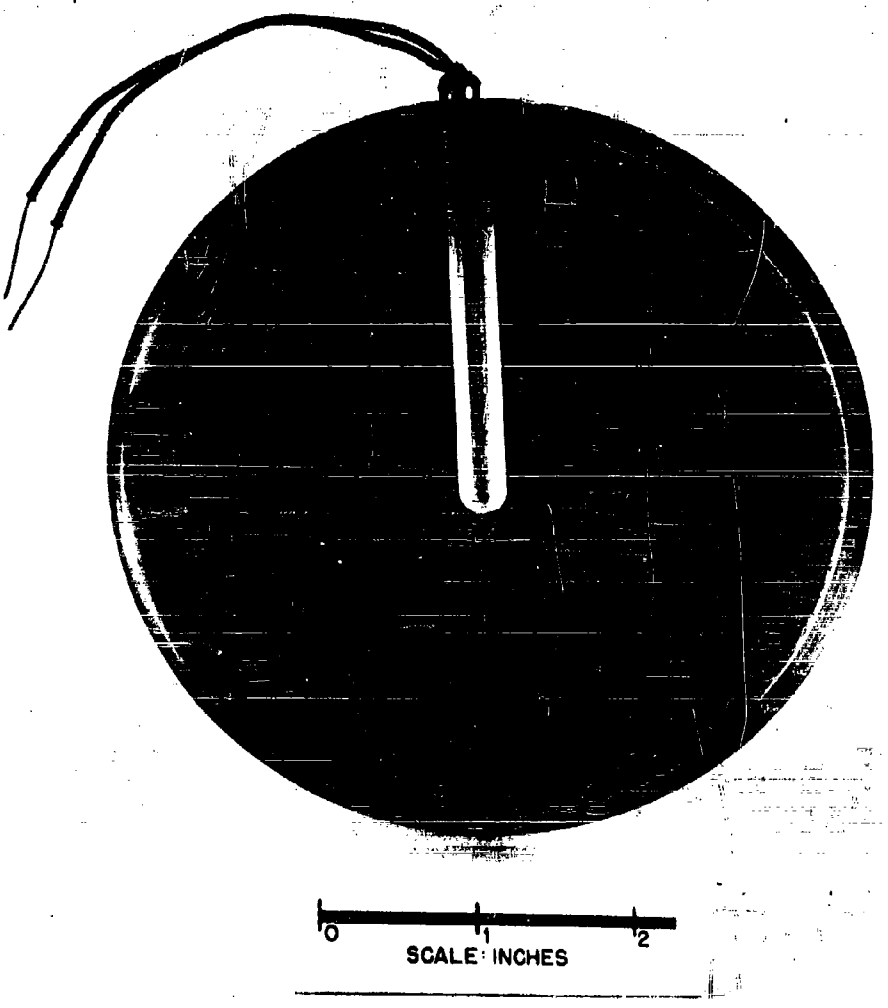

FIG. 2 HEMISPHERE CONFIGURATION: HEAD-ON VIEW (WAX CHARGE)

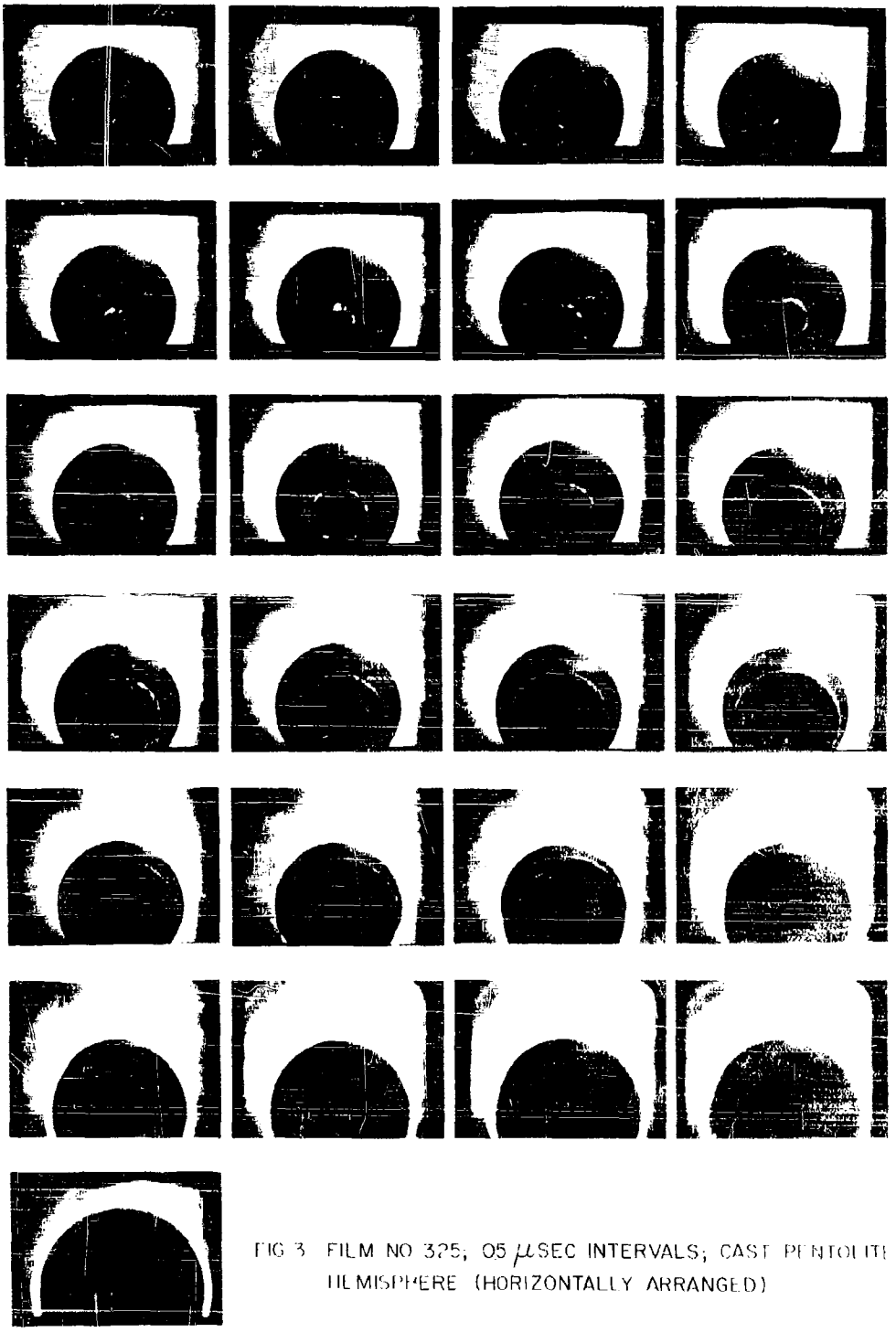

FIG 3 FILM NO 325; 05 μSEC INTERVALS; CAST PENTOLITE
HEMISPHERE (HORIZONTALLY ARRANGED)

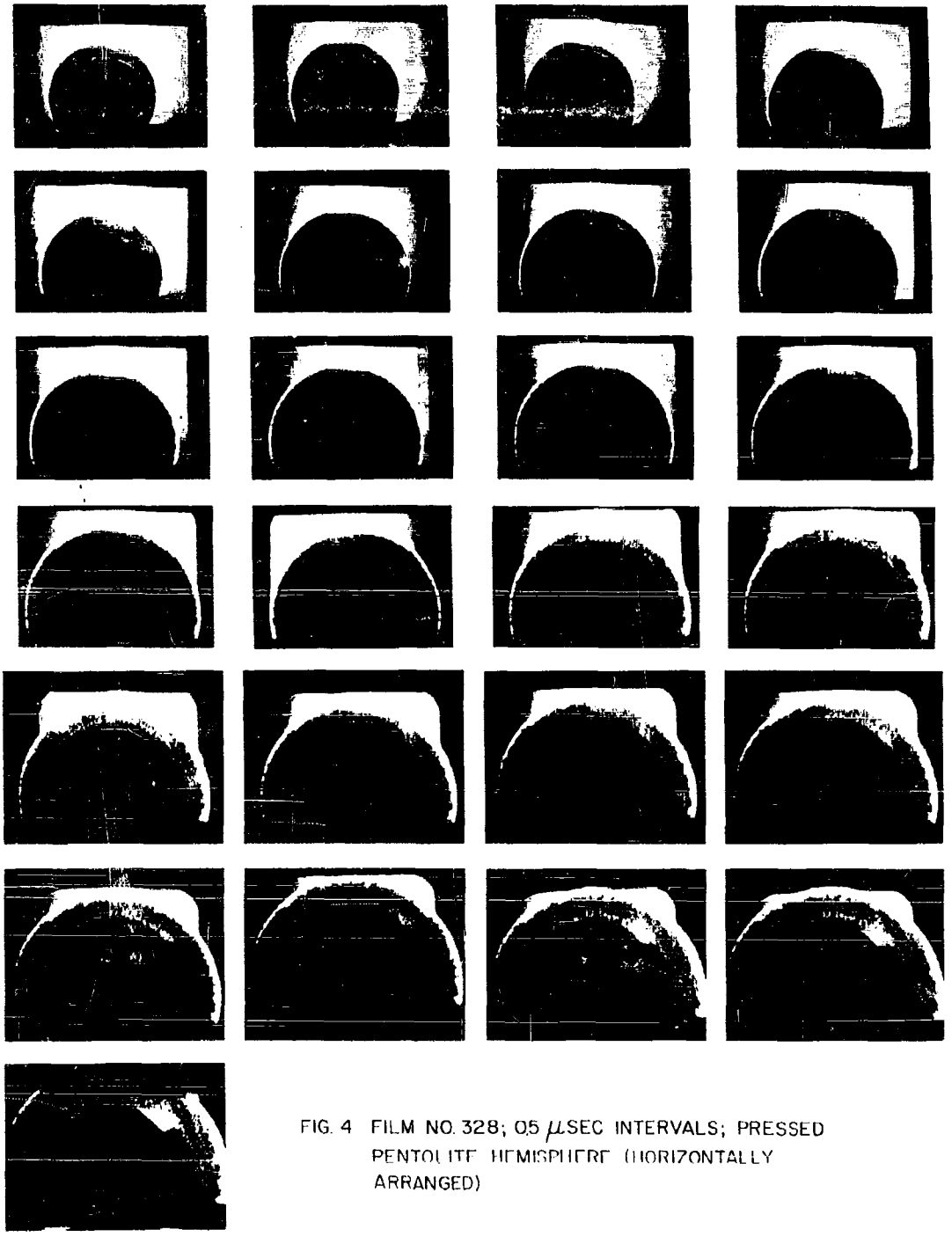

FIG. 4 FILM NO. 328; 0.5 μSEC INTERVALS; PRESSED PENTOLITE HEMISPHERE (HORIZONTALLY ARRANGED)

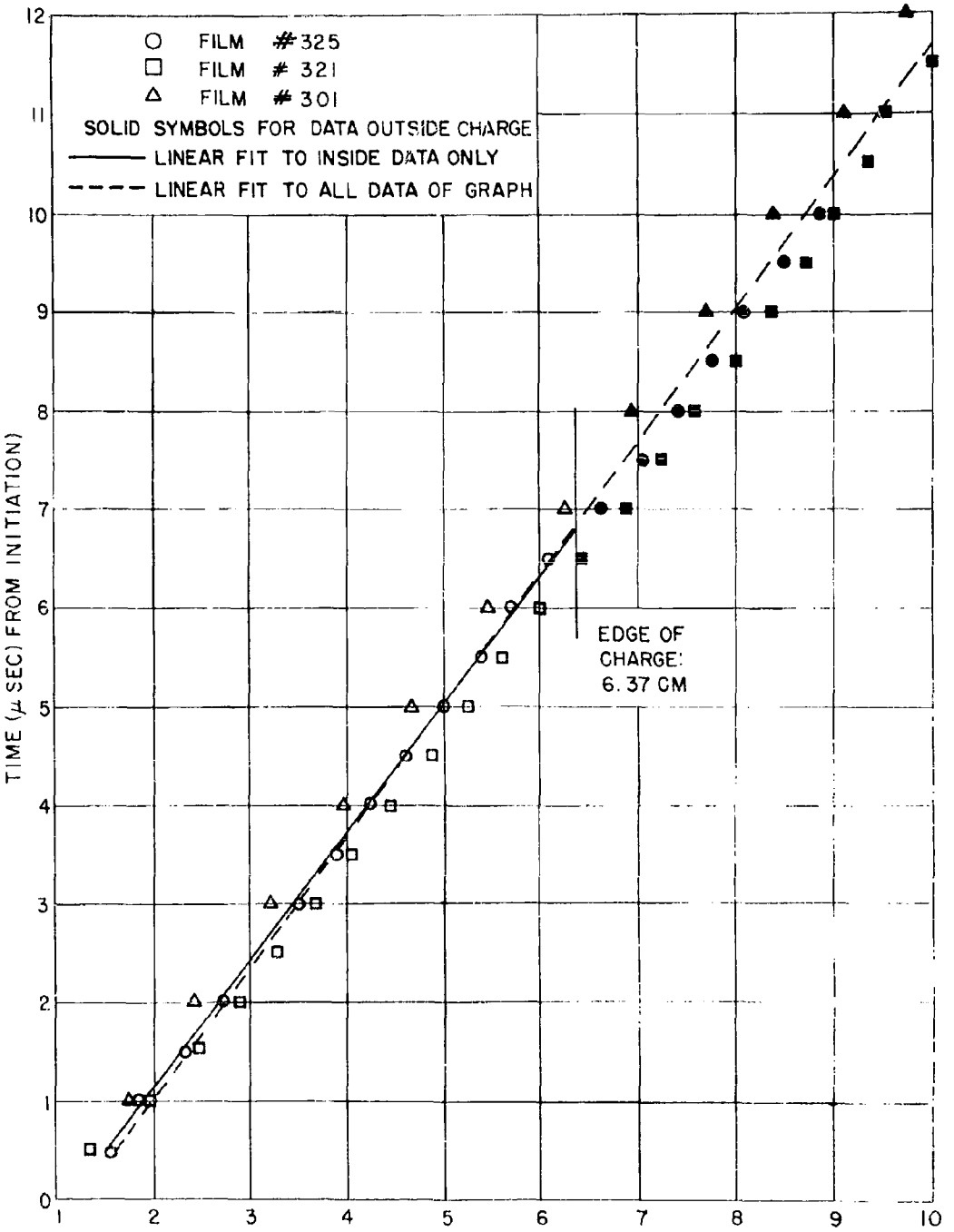

FIG.5 RADIUS-TIME INSIDE CHARGE

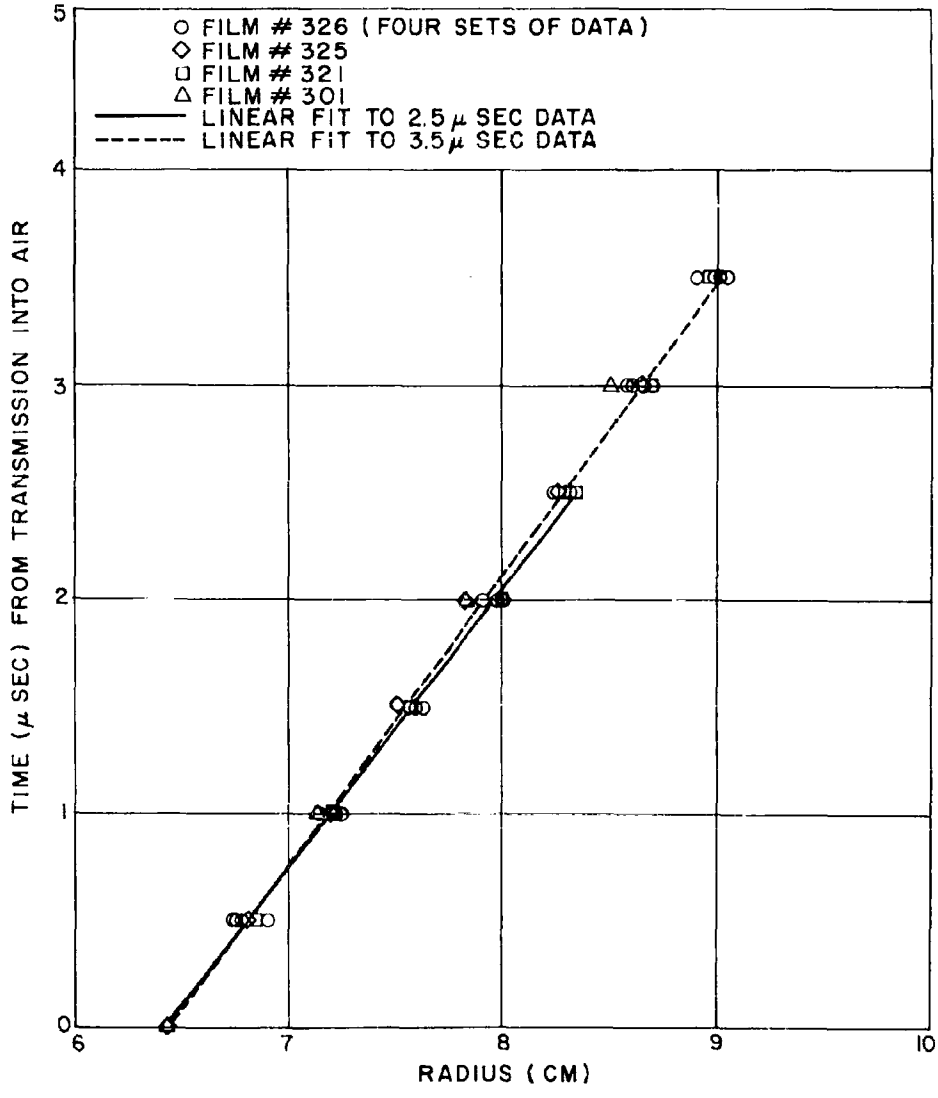

FIG. 6 CLOSE-IN RADIUS-TIME IN AIR

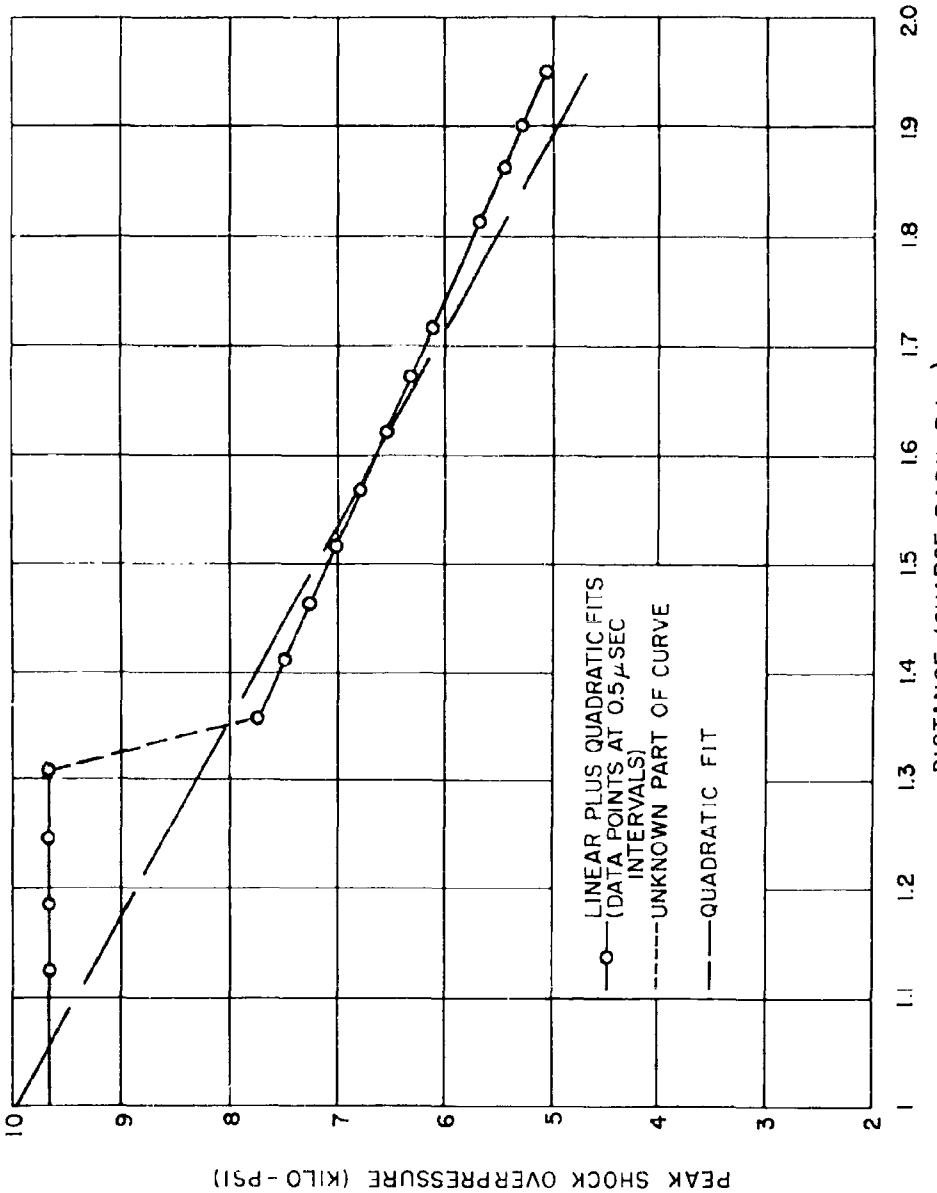

FIG.7 PRESSURE-DISTANCE FOR CAST PENTOLITE HEMISPHERES

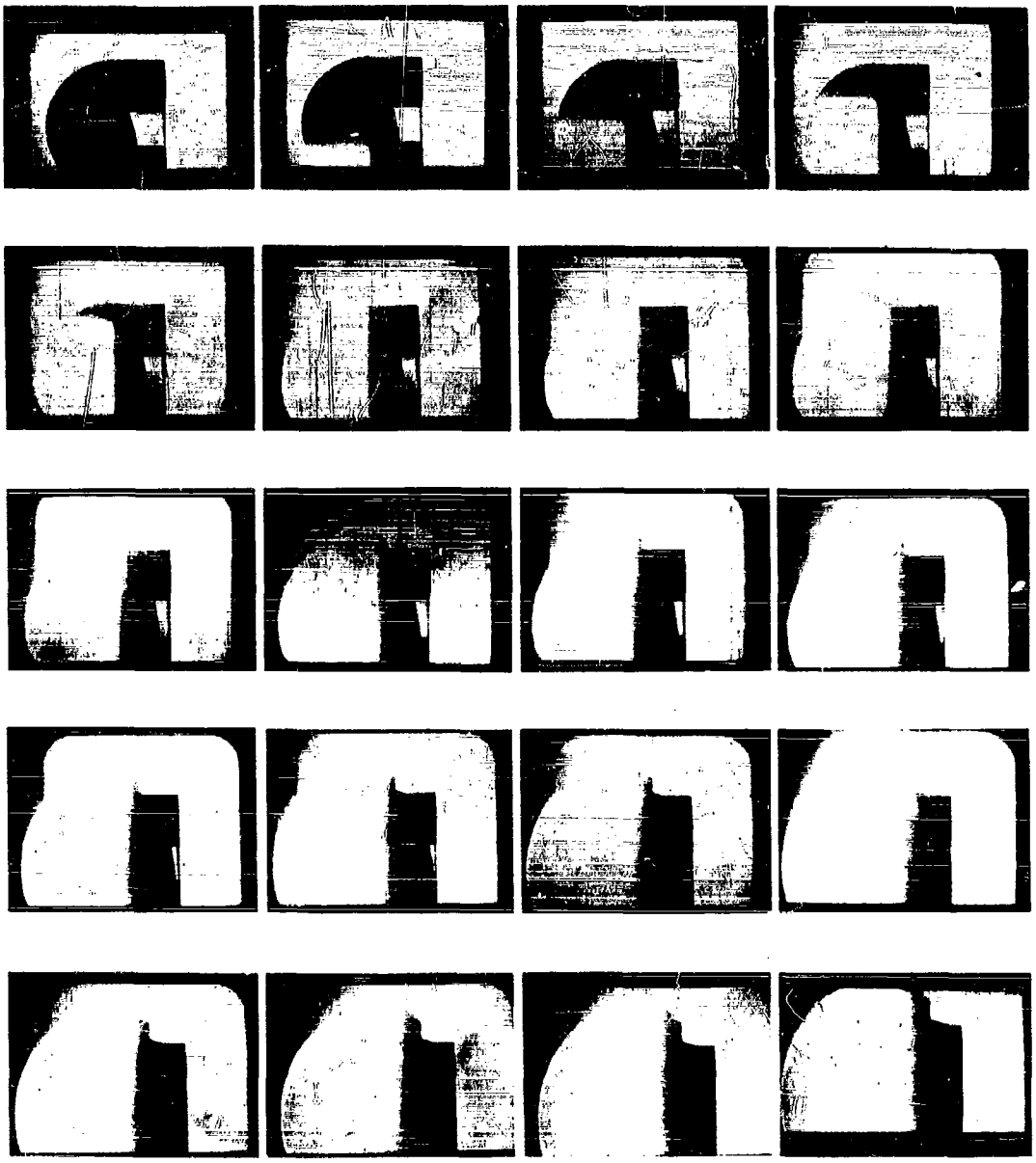

FIG. 8 FILM NO. 326; 0.5 μSEC INTERVALS; CAST PENTOLITE HEMISPHERE (HORIZONTALLY ARRANGED)

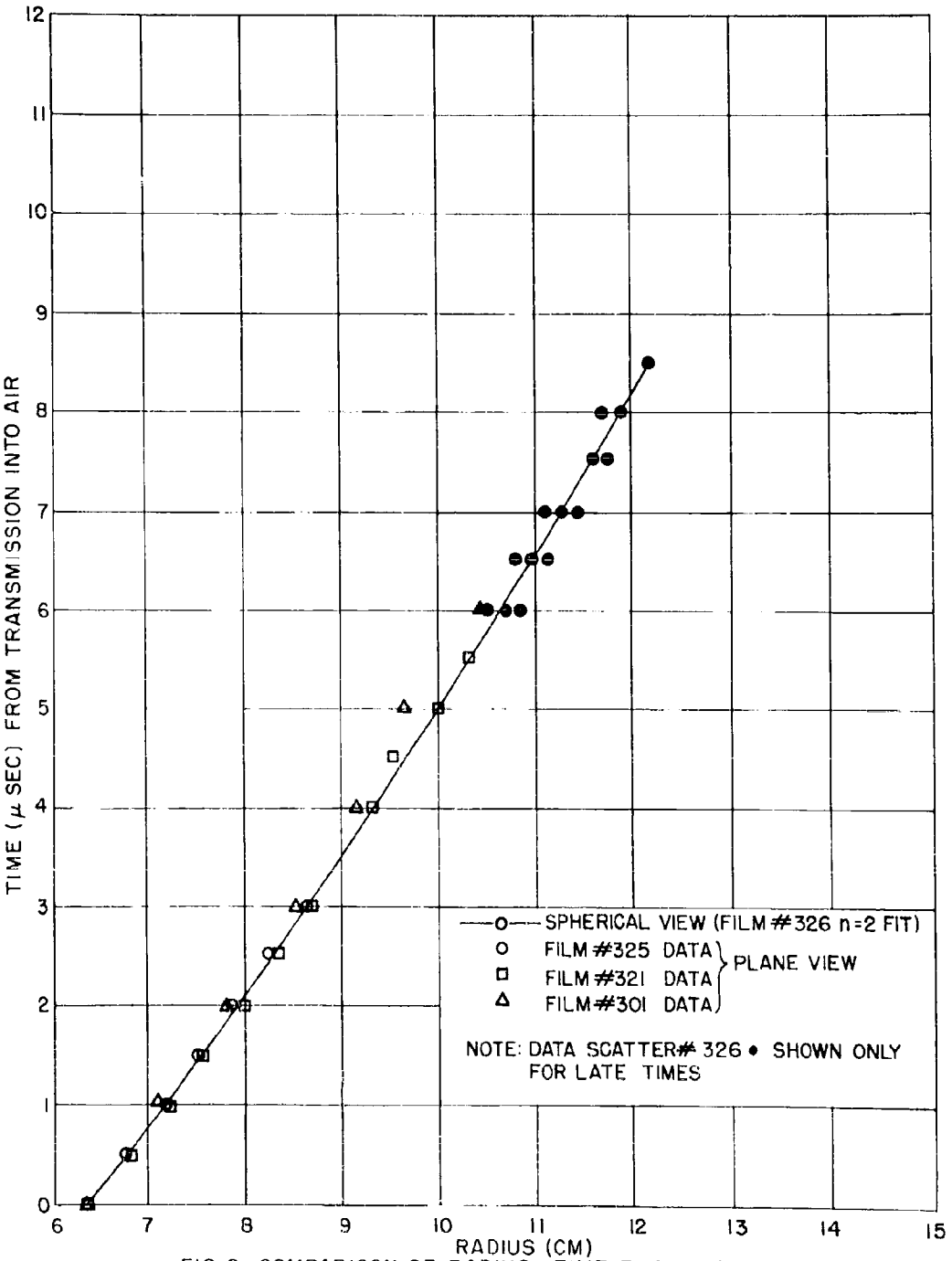

FIG. 9 COMPARISON OF RADIUS-TIME FROM CAST PENTOLITE: PLANE AND SPHERICAL VIEW

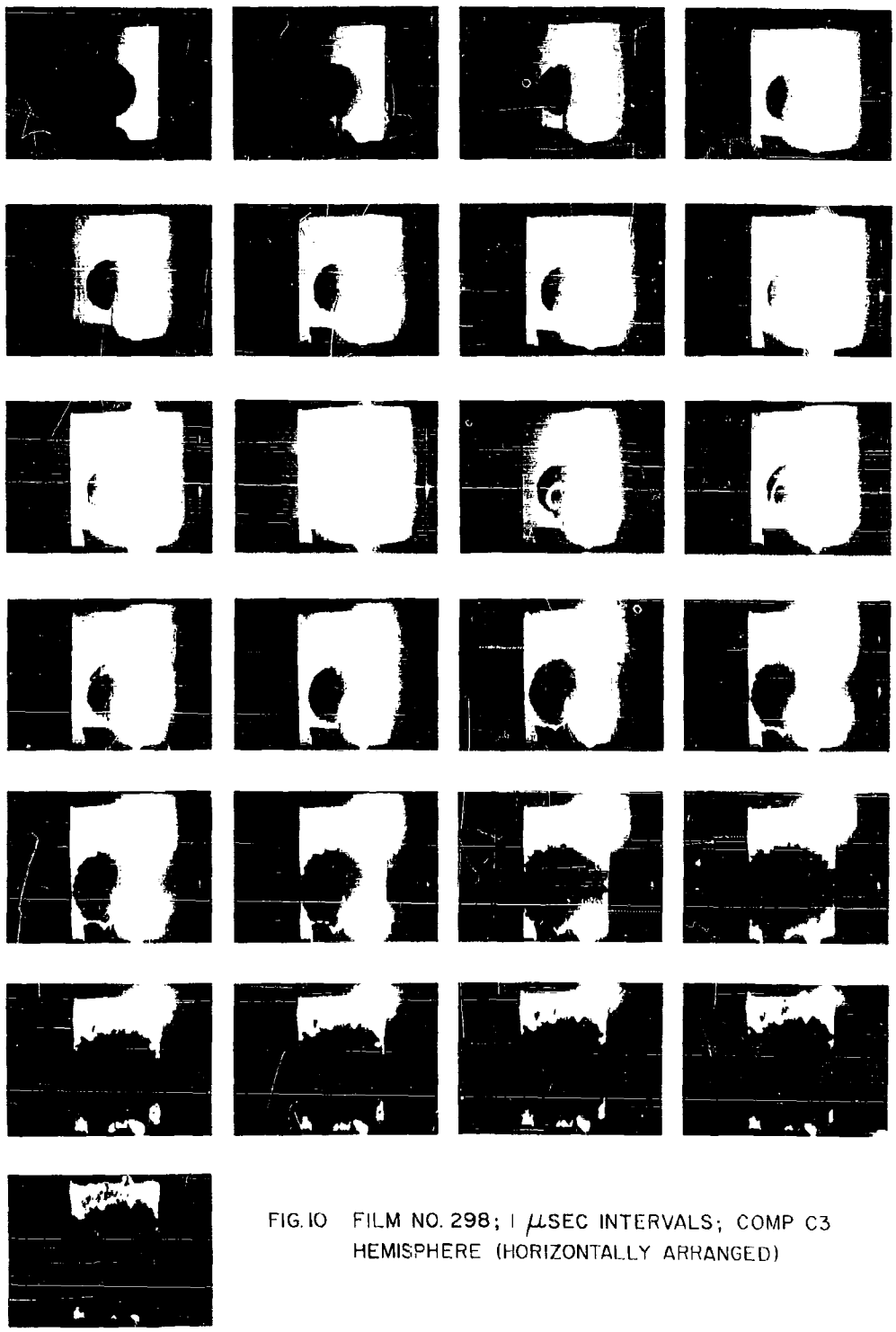

FIG. 10 FILM NO. 298; 1 μSEC INTERVALS; COMP C3 HEMISPHERE (HORIZONTALLY ARRANGED)

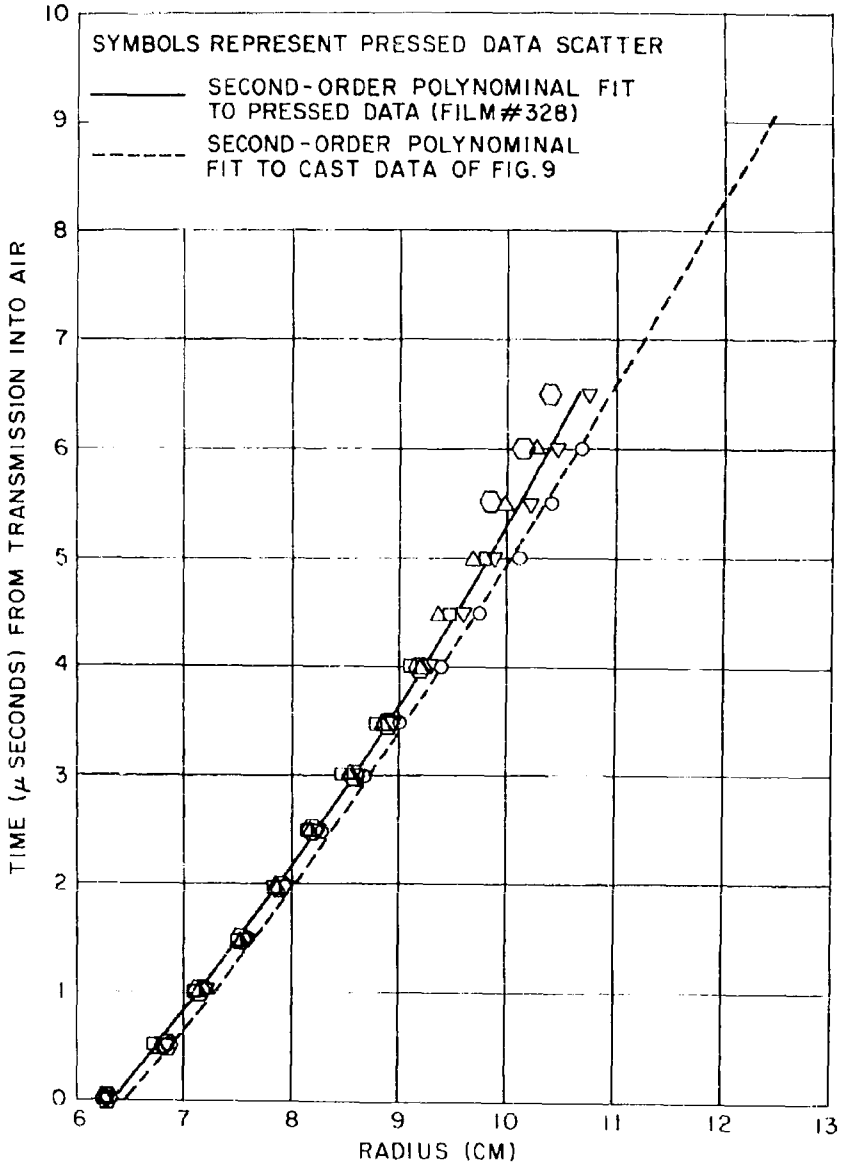

FIG. 11 RADIUS-TIME OUTSIDE PRESSED AND CAST PENTOLITE HEMISPHERES

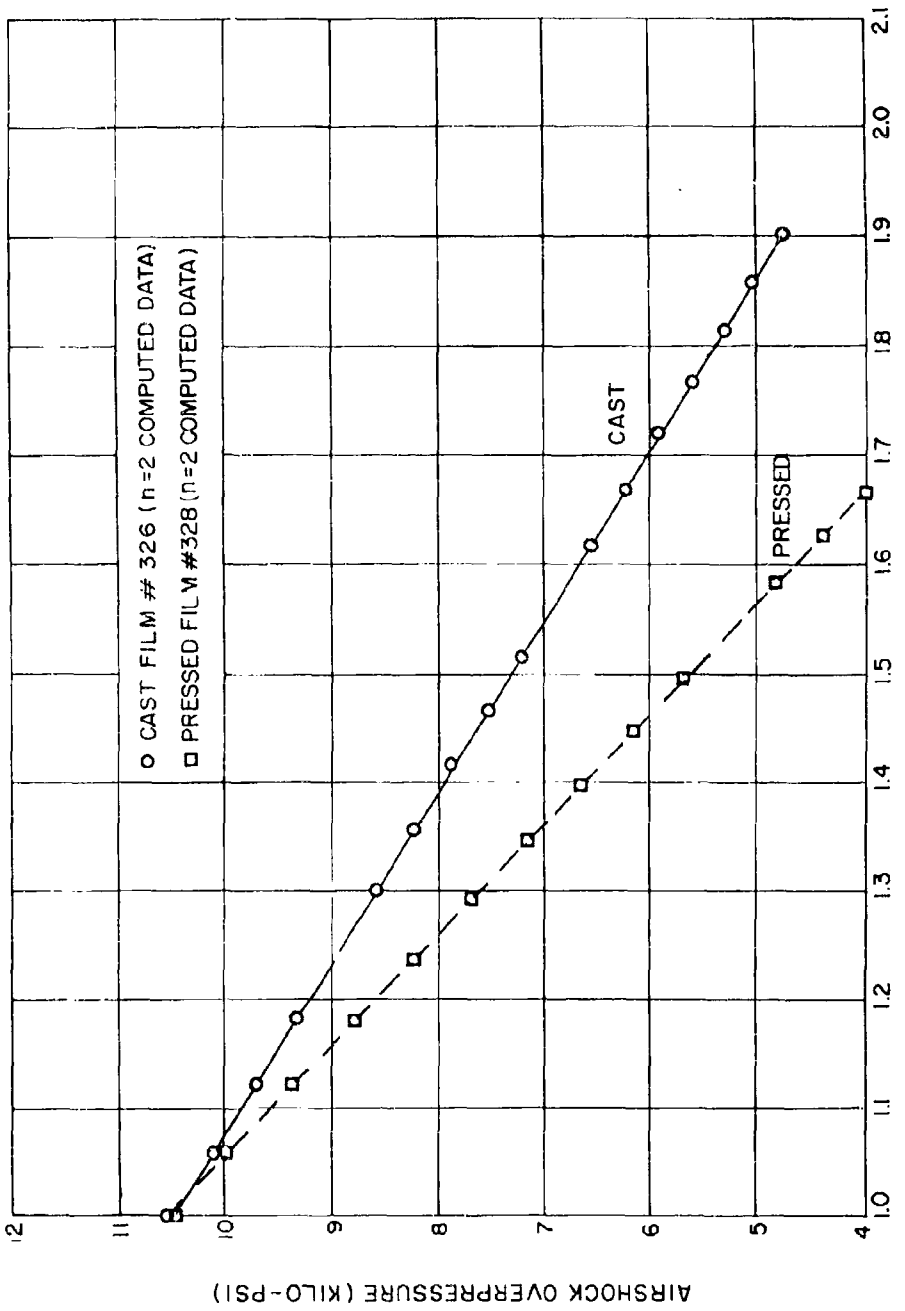

FIG. 12 PRESSURE-DISTANCE CURVES FOR CAST AND PRESSED PENTOLITE HEMISPHERES

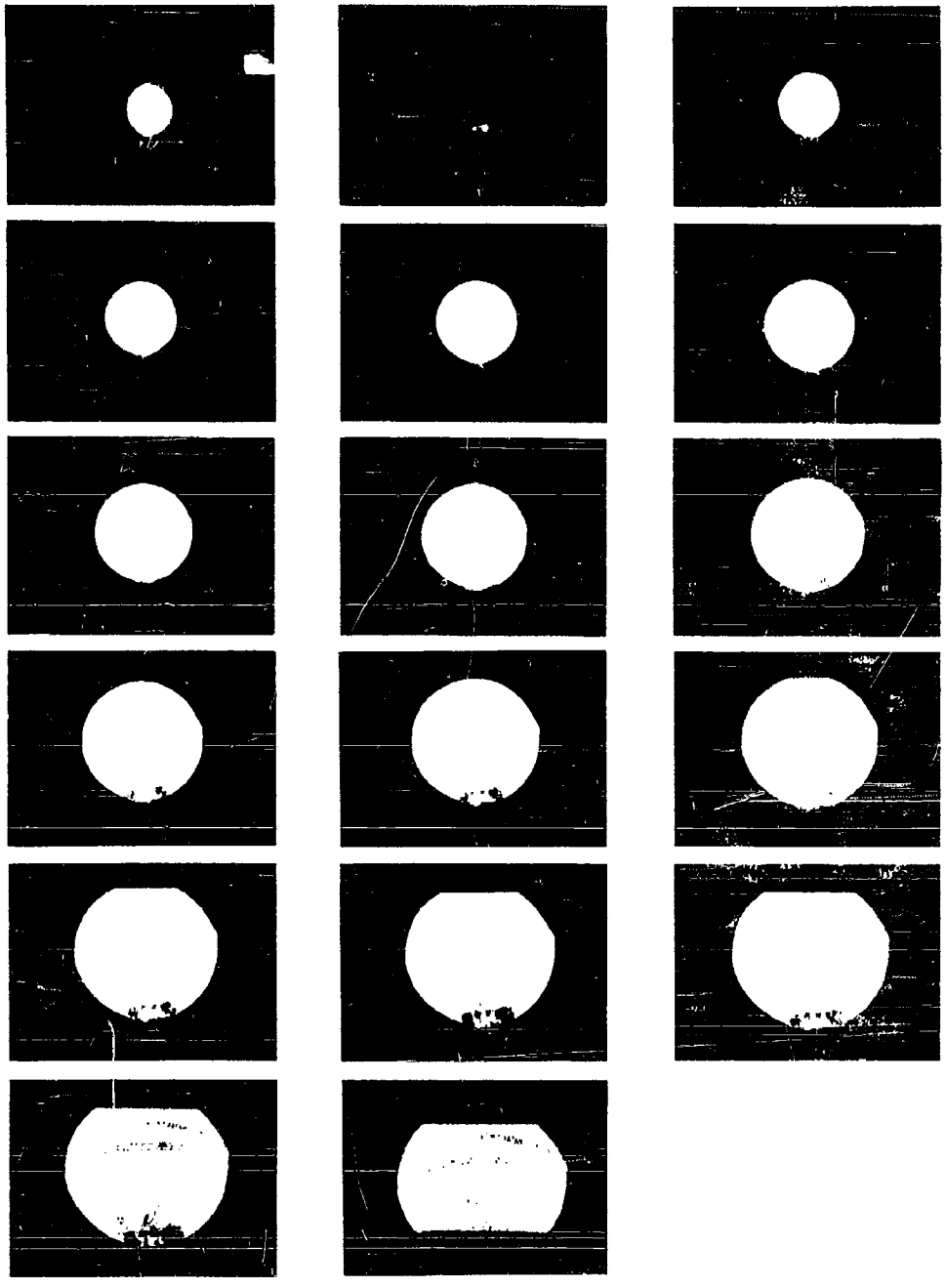

FIG.13 FILM NO. 118; 1 μSEC INTERVALS; CAST PENTOLITE SPHERE (HORIZONTALLY ARRANGED)

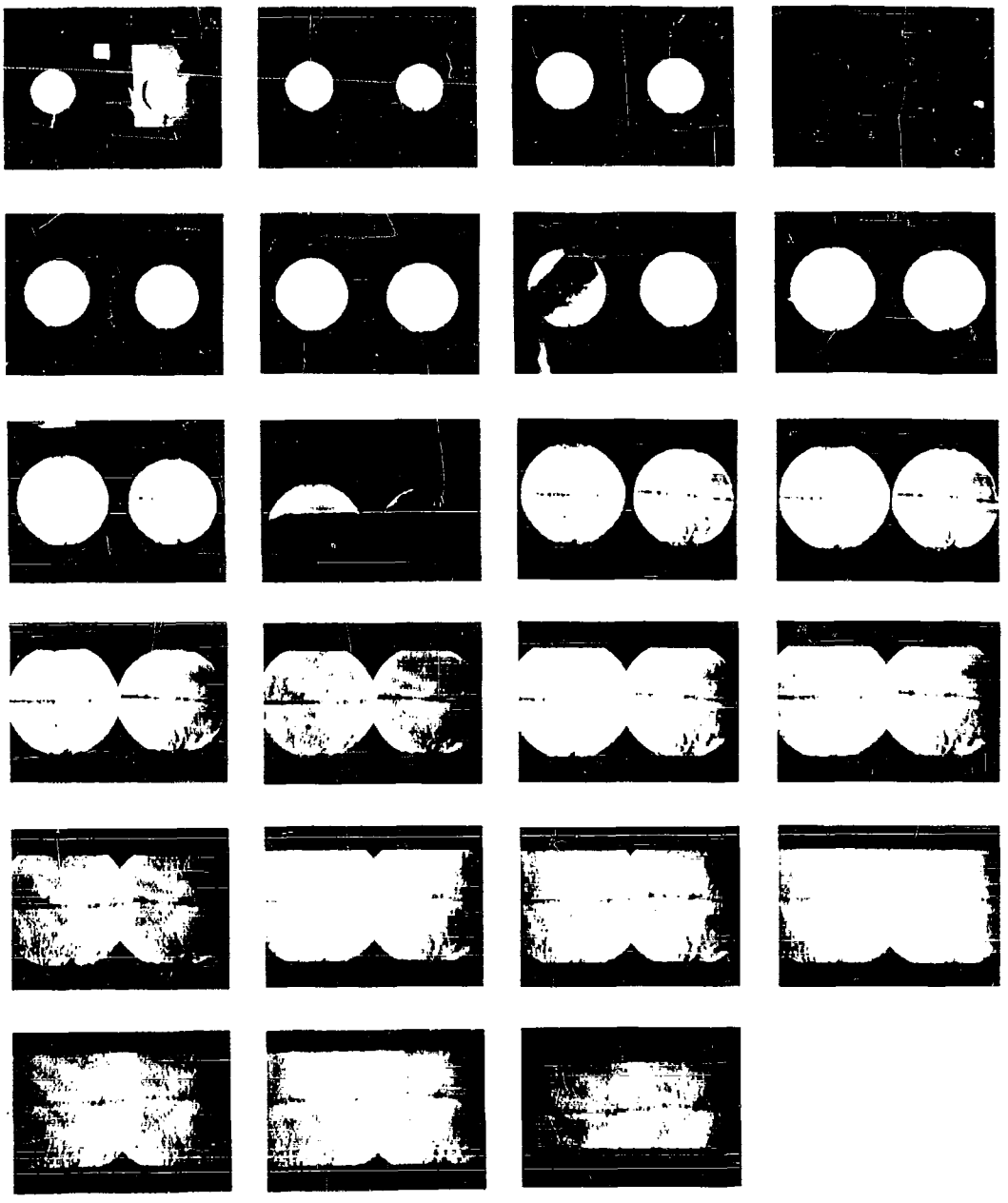

FIG. 14 FILM NO. 120; 1 μSEC INTERVALS; CAST PENTOLITE SPHERE (HORIZONTALLY ARRANGED)

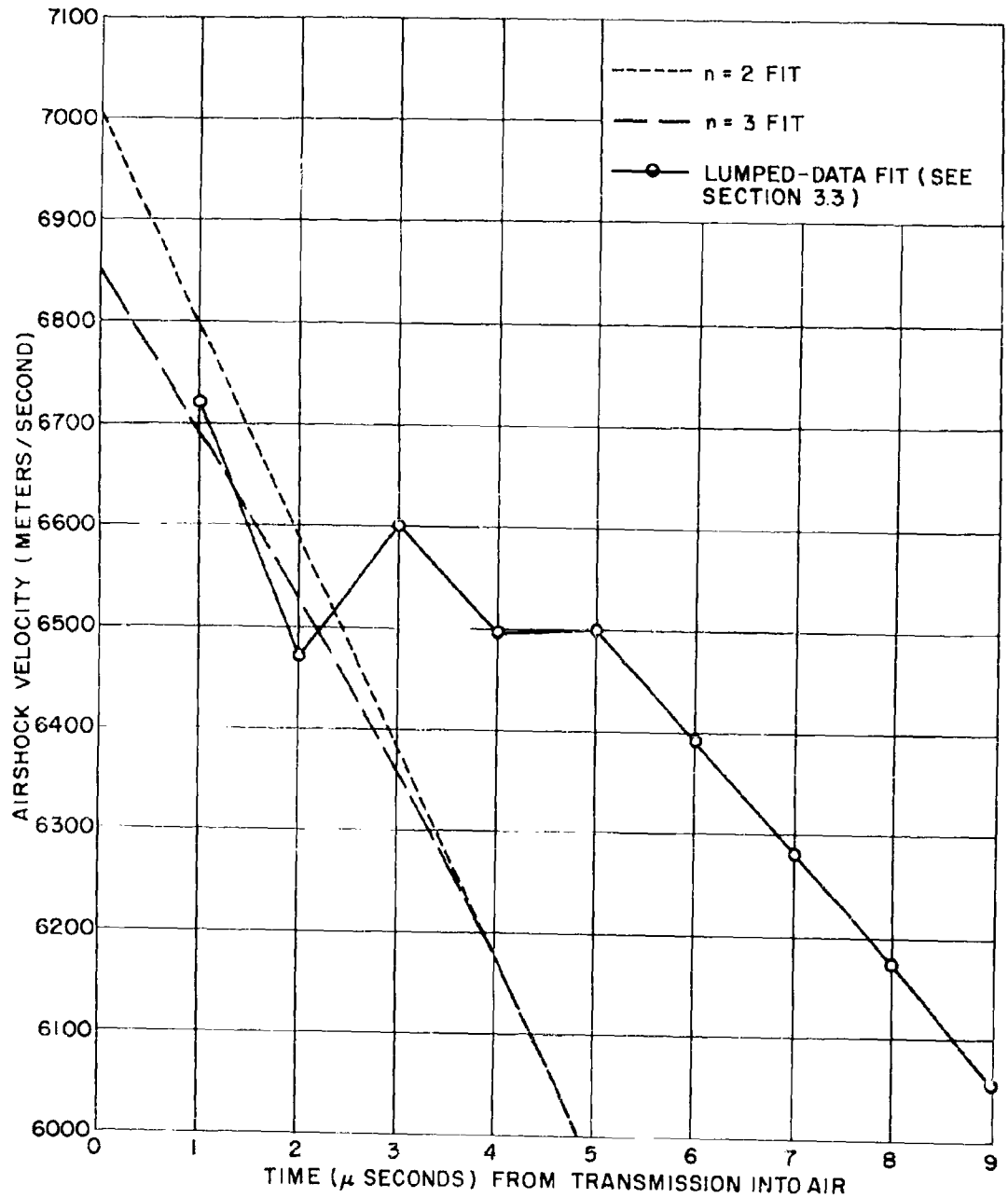

FIG. 15 PENTOLITE SPHERES: AIRSHOCK VELOCITY VS TIME

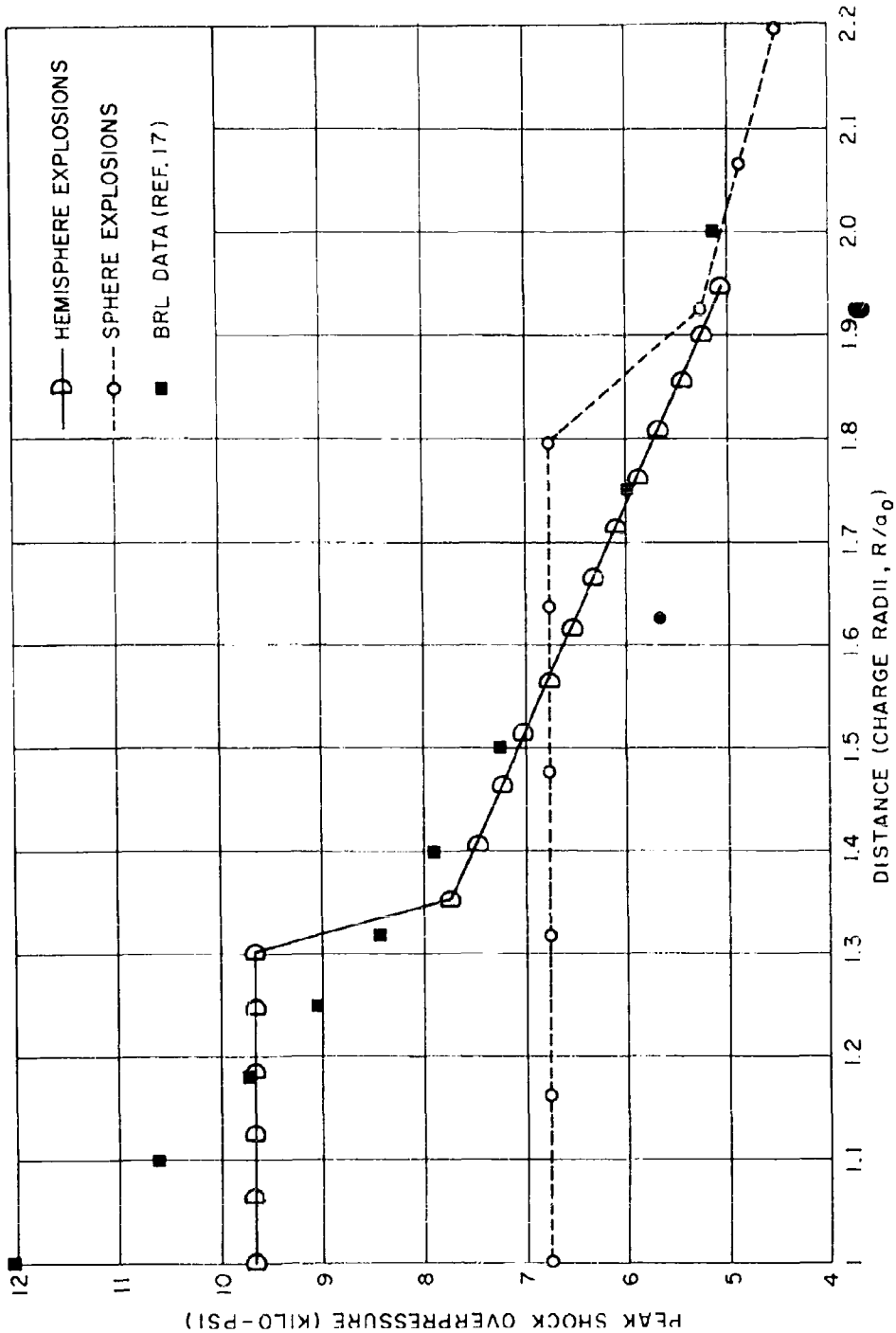

FIG.16 SUMMARY PRESSURE-DISTANCE CURVES FOR CAST PENTOLITE EXPLOSIONS

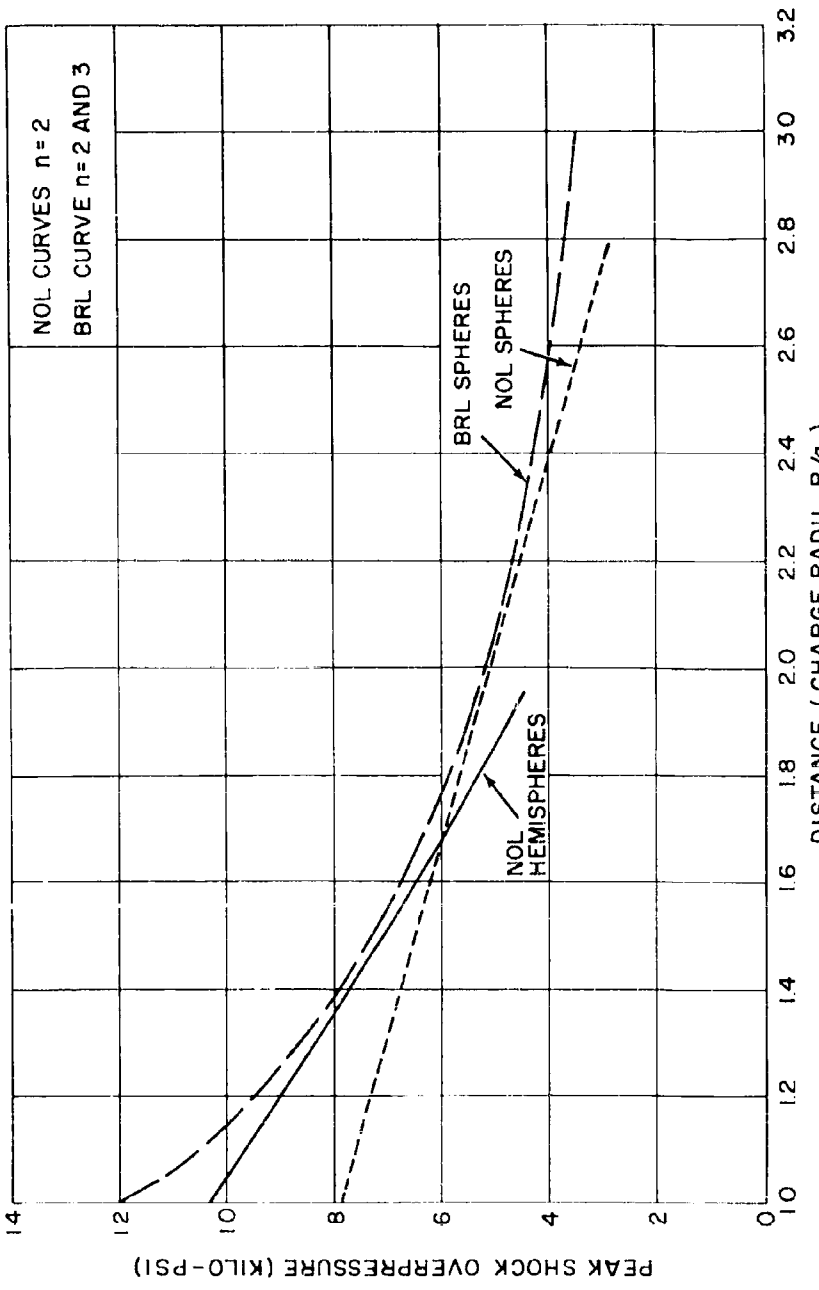

FIG. 17 COMPARISON OF POLYNOMIAL PRESSURE-DISTANCE CURVES: CAST PENTOLITE

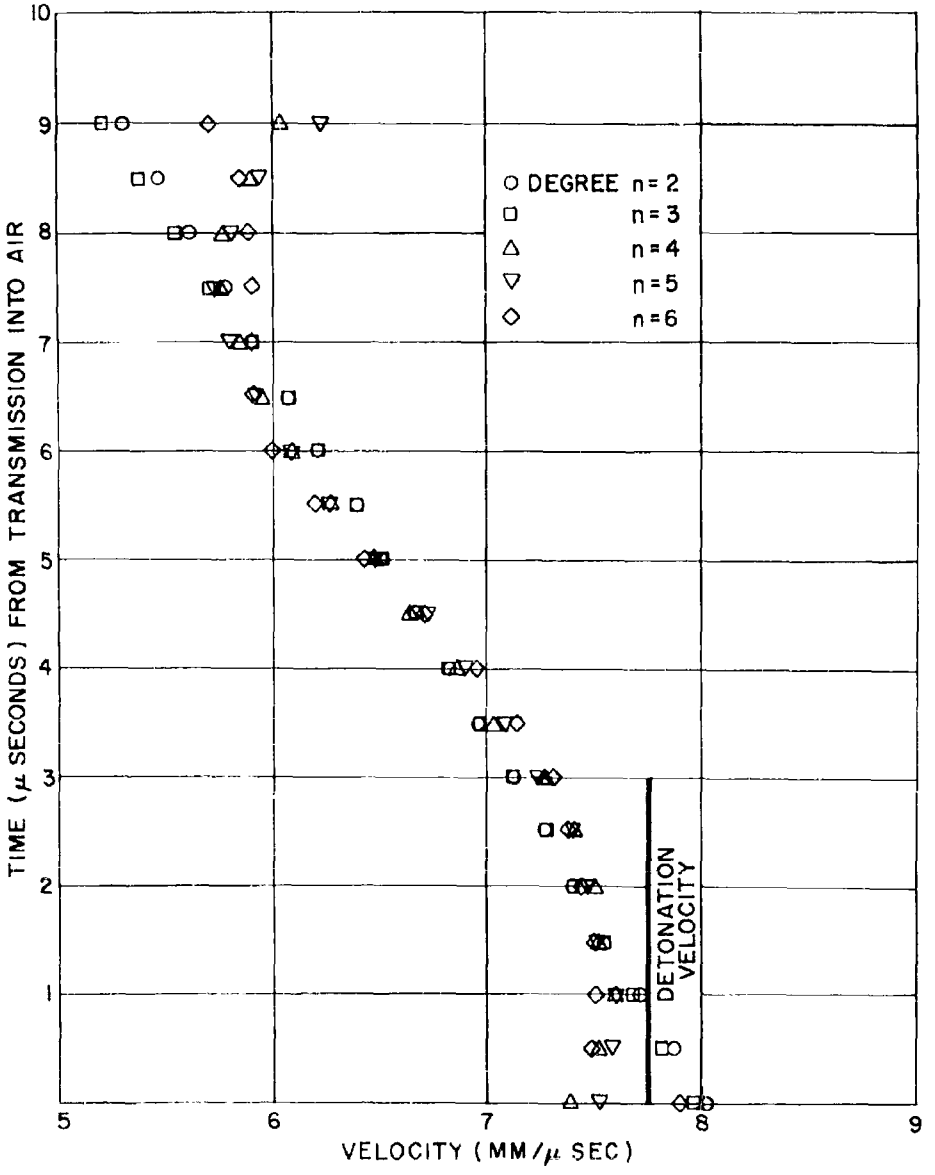

FIG. 18 COMPARISONS OF VELOCITIES FROM VARIOUS POLYNOMINALS FITTED TO AIRSHOCK DATA OF FILM # 326

APPENDIX A

Numerical Procedures

Photographic measurements of explosion phenomena supply only data for the distance-time relation of the phenomena that are observed. In order that these data be useful for producing velocity, and then pressure, the experimental data must be differentiated in some fashion. In so doing lies a serious problem: the procedure for differentiation is not unique. The radius-time data themselves can be fitted by any number of mathematical, or even theoretical, expressions with great precision. But this goodness of fit is hardly important. When the differentiation is made to determine velocity, the curve that is fitted will be differentiated and we cannot obtain a "true" velocity. Several fitting functions may produce fits to the distance-time data that are almost identical but the derivatives of those functions may be very different. This difficulty in obtaining the velocity of an airshock is made worse when the pressure is computed from the Rankine-Hugoniot formula, since the pressure is proportional to the square of the velocity. (These problems, and others, are discussed in detail in Reference (18). The computations of this report were made by Mr. D. L. Lehto, using the machine programs of Reference (18) on the IBM-7090 computer.)

Over a period of years (and unhappiness with the confusion), we in the Air-Ground Explosions Division have reconciled ourselves to the following procedure for most data-reduction problems.

Polynomials of the form

$$r = C_0 + C_1 t + C_2 t^2 + \ldots\ldots\ldots\ldots + C_n t^n$$

where r is the distance, usually radius

t is the time
n is the highest degree of the polynomial

are fitted to the photographic r - t data for values of n usually from n = 2 to n = 6 and differentiated. The velocities from the set of polynomials are then compared with each other to determine whether there is any consistency. The judgment of the scientist must then be invoked to determine which is the best polynomial fit. This judgment, of course, is aided by either other experimental data (such as pressure-gage data) or past experience, or both. Usually the selection can be made on a reasonable basis, particularly for experimental data similar to that from previous experiments. The doubt sets in for new experiments, or for old ones in which one suspects some perturbation may have occurred. The main point is, however, that the numerical procedure is never cut-and-dried and must always be related to the judgment of the data-processor.

In Figure 18 we have plotted the situation for Film 326 as an example characteristic of the data of this report. Polynomial fits from n = 2 to n = 6 were made to the four sets of r - t data obtained from Film 326. The average errors (the average error is defined as the arithmetic average of the deviations of experimental distances from the polynomial distances at fixed times) for the polynomial fits were:

n	average error (per cent)
2	0.827
3	0.831
4	0.840
5	0.837
6	0.836

From these errors one would conclude that the fits were uniformly good. But from Figure 18 one realizes that the errors are meaningless. In Figure 18 we have plotted the computed velocity at each time value of the data. This scatter in the velocity, of course, becomes enlarged when pressure is computed.

As noted in the text, we have interpreted, necessarily, the data as we understood the phenomena that were occurring. This has resulted in the constant-velocity region discussed in the text; in the decaying region n = 2 polynomial fits have generally been used.

APPENDIX B

Conditions at the Explosive-Air Interface

B-1. The Boundary Conditions: We discuss here the requirements at the boundary of the explosive and indicate why we cannot complete the transmission formulas.

In our model of the explosion, we assume that a shock exists in the explosive and is transmitted into the air to create the airshock. Across the shock in the explosive just before the shock reaches the boundary of the explosive, we write the usual stationary plane-wave relations for conserving mass and momentum:

$$\rho_o' \, D = \rho' \, (D-u') \tag{1}$$

$$p' - p'_o = \rho_o' \, u' \, D \tag{2}$$

where

ρ_o' = undisturbed explosive density

ρ' = density at the detonation shockfront in the explosive

u' = particle velocity at the detonation shockfront

p' = pressure at the detonation shockfront

p'_o = local ambient pressure in the explosive

D = velocity of the detonation shockfront

On the other side of the sharp explosive boundary we assume that a shock exists in the air, and write:

$$\rho_o D = \rho \, (U-u) \tag{3}$$

$$p-p_o = \rho_o u \, U \tag{4}$$

where the unprimed symbols apply to the airshock or velocity U. Since we know that the pressures p and p' are large, we neglect p_o in both (2) and (3) and subtract

$$p-p' = \rho_o u \, U - \rho_o' \, u'D \tag{5}$$

We have gone about as far as we can go. If we could assume that burning had ceased in the detonation wave so that $p = f(\rho, S) = f(\rho)$ only, (where S is the entropy) then we could write for the rarefaction wave moving back into the detonation wave (of finite reaction-zone width) the usual Riemann relation

$$u'_2 = u' + \int_{\rho'_2}^{\rho'} C' \frac{dp'}{\rho'}$$

for an isentropic medium where C' is the sound speed. If this were true, we could invoke the continuity of pressure and particle velocity at the interface so that $u'_2 = u$ and $p'_2 = p$, where the subscript 2 refers to data at that place where the rarefaction wave has moved back from the explosive interface to the center of the explosion. If we were to assume that the usual adiabatic relations apply to the detonation wave zone which has been swept by the rarefaction wave, then we could find that the integration is easily performed and results in

$$u'_2 = u' + \frac{2}{\gamma'-1}\sqrt{\frac{\gamma' p'}{\rho'}}\left[\, 1 - \left(\frac{p'_2}{p'}\right)^{\frac{\gamma'-1}{2\gamma'}} \,\right] \qquad (6)$$

which may be used in (5), along with the usual shock formulas for ρ, D, etc. This procedure has already been done by Pack (Ref. (8)) among others for the assumptions cited - isentropocity and adiabaticity of the medium behind the rarefaction wave - when the reaction-zone behind the detonation shockfront is ignored or set equal to zero.

Since it is quite clear to us that the finite reaction-zone width must be considered and that the above assumptions are not correct, we must know the details of the rarefaction wave - reaction zone reactions to write the correct equations, if the explosive-air interface is a sharp boundary. If, indeed, the burning of explosive grains does continue into the air to support the airshock motion at constant velocity for a finite time, then the situation to be described becomes even more involved. Perhaps one must surrender the formulation of the correct transmission relations and seek a theoretical description which avoids explicit description of these relations.

B-2. Although we cannot write down the correct equations across the explosive-air interface, we can examine, crudely, the transmission using the experimental results. Let us ask a specific question, as an example: Can the airshock velocity exceed the detonation-shock velocity?

Let us assume that a sharp boundary between explosive material and the air exists. At the moment of collision of the detonation shock with the boundary, we assume that the shock relations (1) and (3) hold on either side of the boundary. If we solve these equations for the shock velocities D and U and form the ratio, we have

$$\frac{U}{D} = \frac{u}{u'} \frac{1 - \frac{\rho_0'}{\rho'}}{1 - \frac{\rho_0}{\rho}} \quad . \tag{7}$$

We can estimate the values of the density ratios and obtain a relation between the front- and the particle-velocity ratios. From tabular data on the equation of state of air at 8,000 to 10,000 psi, we find that $\rho/\rho_0 \sim 12$ so that $(1 - \rho_0/\rho) \sim 11/12$. For the density ratio inside the explosive material, several estimates are possible; we consider two possible values. If we assume

$$\frac{\rho_0'}{\rho'} = \frac{\gamma' - 1}{\gamma' + 1} , \tag{7'}$$

then this ratio is 1/2 for $\gamma' = 3$ (cf., Ref. (1)). If we assume that the pentolite value is not too far from that of TNT that we have computed in Reference (3), then $\rho'/\rho_0' = 7/5$. Using the values of 1/2 and 7/5 for the ratios, we find that (7) becomes:

$$\frac{U}{D} = \frac{12}{22} \left(\text{or } \frac{24}{77} \right) \frac{u}{u'}$$

The 12/22 results from the use of $\gamma' = 3$ and the 24/77 from the TNT value. The first fraction, based on $\gamma' = 3$, could be considered to result from the picture of the detonation wave in which the reaction-zone thickness is zero, since the $\gamma' = 3$ value should hold for the reaction product gases. The TNT fraction, 24/77, on the other hand, is based on the calculated results of Reference (3) for the density ratio within the reaction zone. One should not conclude that these two fractions bound the range of possible values; they are merely two possible estimates.

To find the particle-velocity ratio in (7'), we use the fact that $u_2' = u$ when the rarefaction wave is set up at the sharp interface and assume the validity of equation (6) to describe the particle velocity for either explosive or air. If we use $\gamma' = 3$ for the gases in the assumed adiabatic, isentropic flow described by (6), we find

$$u_2' = u = u' + \sqrt{\frac{3\,p'}{\rho'}} \left[1 - \frac{\rho_2'}{\rho'} \right] = u' + (D - u') \left(1 - \rho_2'/\rho'\right) , \tag{8}$$

if we note $\sqrt{\frac{3p'}{\rho'}} = C'$ and assume $C' = D - u'$, the Chapman-Jouguet condition for the flow. To find the density ratio after and before the rarefaction wave ρ_2'/ρ', we have experimentally that $p' \sim 3 \times 10^5$ psi for a typical detonation pressure of the pentolite shockfront and $p \sim 1 \times 10^4$ psi from our air data of this report. Thus, since $p_2' = p$, by continuity, we have

$$\frac{p_2'}{p'} = \frac{10^4}{3 \times 10^5} = \frac{1}{300}$$

hence: $$\frac{\rho_2'}{\rho'} = \left(\frac{p_2'}{p'}\right)^{\gamma'} \simeq \frac{1}{7} \text{ for } \gamma' = 3.$$

Using this in (8), we find ($u_2' = u$):

$$\frac{u}{u'} = \frac{1}{7} + \frac{6}{7}\frac{D}{u'} \quad . \tag{9}$$

But from (1) we have

$$\frac{D}{u'} = \frac{1}{1 - \rho_o'/\rho'}$$

which equals 2 for $\gamma' = 3$ and equals 7/2 from the TNT results. Using this ratio in (9) and the result in (7') gives:

$$\text{(TNT):} \quad \frac{U}{D} = \frac{24}{77} \times \frac{22}{7} = 0.979$$

$$(\gamma' = 3): \quad \frac{U}{D} = \frac{12}{22} \times \frac{13}{7} = 1.013$$

as two values of the shock-velocity ratio. Now, in (8), we used the relation $D = u' + C'$, which relation holds when the reaction-zone thickness is zero. If we want to consider the finite reaction-zone thickness results of Reference (3) for TNT, we find $2.5D = u' + C'$.

If we make only this one change in the previous arithmetic, we find:

(TNT): $\frac{U}{D} = 2.38$

($\gamma' = 3$): $\frac{U}{D} = 2.41$.

These last values appear unreasonably high; at least our data do not permit an interpretation of the initial airshock velocity as 2.4 times greater than the detonation velocity.

Our arithmetic, for the case $D = u' + C'$, then gives us the result that the initial airshock velocity is approximately equal to the detonation velocity, which result appears compatible with our interpretation of the experimental data.

DISTRIBUTION

ARMY	Copies
Chief of Research and Development, D/A, Washington 25, D. C. Attn: Atomic Division	1
Chief of Engineers, D/A, Washington 25, D. C. Attn: ENGCW-NE, ENGTE-E, ENGMC-E	3
Commanding General, U.S. Army Materiel Command, Washington, D. C. Attn: AMCRD-DE-N	2
Commanding General, U.S. Continental Army Command, Ft Monroe, Va.	1
President, U.S. Army Air Defense Board, Ft Bliss, Texas	1
Commandant, Command & General Staff College, Ft Leavenworth, Kansas Attn: Archives	1
Commandant, U.S. Army Air Defense School, Ft Bliss, Texas Attn: Command & Staff Dept	1
Director, Special Weapons Development, Hq CDC, Ft Bliss, Texas Attn: Chester I. Peterson	1
Commanding General, Aberdeen Proving Ground, Aberdeen, Maryland Attn: BRL for Director, J. J. Keszaros, W. J. Taylor, R. E. Shear	4
Commanding General, The Engineer Center, Ft Belvoir, Virginia Attn: Asst Commandant, Engineer School	1
Director, U.S. Army Research and Development Laboratory, Ft Belvoir, Virginia, Attn: Chief, Tech Support Branch	1
Commanding Officer, U.S. Army Mobility Command, Center Line, Michigan	1
Commanding Officer, Picatinny Arsenal, Dover, N. J. Attn: ORDBB-TK	1
Commanding Officer, Transportation Research Command, Ft Eustis, Va. Attn: Chief, Tech Info Div	1
Commanding General, USA Electronic R&D Lab, Ft Monmouth, N. J. Attn: Technical Documents Center, Evans Area	1

ARMY CONT'D	Copies
Commanding General, USA Missile Command, Huntsville, Alabama	1
Commanding General, USA Munitions Command, Dover, New Jersey	1
Commanding Officer, U.S. Army Corps of Engineers, Beach Erosion Board, Washington, D. C.	1
Commanding Officer, U.S. Army Nuclear Defense Laboratory, Edgewood Arsenal, Edgewood, Maryland, Attn: Tech Library	1
Director, Waterways Experiment Station, U.S. Army Corps of Engineers, Vicksburg, Mississippi, Attn: Library, John Strange	2
Director, U.S. Army Corps of Engineers, Nuclear Cratering Group, Livermore, California	1

NAVY	
Chief of Naval Operations, ND, Washington 25, D. C.	
Attn: OP-75	2
Attn: OP-03EG	1
Director of Naval Intelligence, ND, Washington 25, D. C. Attn: OP-922V	1
Chief, Bureau of Naval Weapons, ND, Washington 25, D. C.	
Attn: DIS-3	4
Attn: RUME-11	1
Attn: RRRE-5	1
Chief, Bureau of Ships, ND, Washington 25, D. C. Attn: Code 372, Code 423	2
Chief, Bureau of Yards and Docks, ND, Washington 25, D. C. Attn: Code D-400, Code D440	2
Chief of Naval Research, ND, Washington 25, D. C.	
Attn: Code 811	2
Attn: Code 493, Code 418, Code 104	3
Commander-in-Chief, U.S. Pacific Fleet, FPO, San Francisco, Calif.	1
Commander-in-Chief, U.S. Atlantic Fleet, U.S. Naval Base, Norfolk 11, Virginia	1
Commandant of the Marine Corps, ND, Washington 25, D. C. Attn: Code AO3H	4

NAVY CONT'D	Copies
President, U.S. Naval War College, Newport, R. I.	1
Superintendent, U.S. Naval Postgraduate School, Monterey, California	1
Commanding Officer, Nuclear Weapons Training Center, Atlantic, Naval Base, Norfolk 11, Viriginia, Attn: Nuclear Warfare Department	1
Commanding Officer, U.S. Naval Schools Command, U.S. Naval Station Treasure Island, San Francisco, California	1
Commanding Officer, Nuclear Weapons Training Center, Pacific, Naval Station, North Island, San Diego 35, California	2
Commanding Officer, U.S. Naval Damage Control Training Center, Naval Base, Philadelphia 12, Pa. Attn: ABC Defense Course	1
Commander, U.S. Naval Ordnance Test Station, China Lake, California, Attn: Library, R. E. Boyer	2
Commanding Officer & Director, U.S. Naval Civil Engineering Laboratory, Port Hueneme, California, Attn: Code L31	1
Director, U.S. Naval Research Laboratory, Washington 25, D. C. Attn: Library, Dr. Louis F. Drummeter	2
Commanding Officer & Director, Naval Electronics Laboratory, San Diego 52, California	1
Commanding Officer, U.S. Naval Radiological Defense Laboratory, San Francisco, California, Attn: Tech Info Division	1
Commanding Officer & Director, David W. Taylor Model Basin, Washington 7, D. C., Attn: Library	1
Underwater Explosions Research Division, DTMB, Norfolk Naval Shipyard, Portsmouth, Virginia	1
Commander, U. S. Naval Weapons Evaluation Facility, Kirtland AFB, Albuquerque, New Mexico, Attn: Mr. Earl B. Massingill, Jr.	1
Commanding Officer, U. S. Naval Propellant Plant, Indian Head, Maryland, Attn: Technical Library	1

AIR FORCE	Copies
Hq, USAF (AFDRC/NE - Maj Lowry) Washington 25, D. C.	1
Deputy Chief of Staff, Plans and Programs, Hq USAF, Washington 25, D. C., Attn: War Plans Division	1
Director of Research and Development, DCS/D, Hq USAF, Washington 25, D. C., Attn: Guidance & Weapons Division	1
Air Force Intelligence Center, Hq USAF, ACS/I (AFCIN-3K2) Washington 25, D. C.	1
Commander-in-Chief, Strategic Air Command, Offutt AFB, Nebraska, Attn: OAWS	1
Commander, Tactical Air Command, Langley AFB, Virginia Attn: Document Security Branch	1
ASD, Wright Patterson AFB, Ohio	1
Commander, Air Force Logistics Command, Wright-Patterson AFB, Ohio	2
AFSC, Andrews Air Force Base, Washington 25, D. C. Attn: RDRWA	1
Director, Air University Library, Maxwell AFB, Alabama	2
AFCRL, L. G. Hanscom Field, Bedford, Massachusetts Attn: CRQST-2, H. P. Gauvin	2
AFWEL (SWRS) Kirtland AFB, New Mexico Attn: Maj A. Deptula	1
Commandant, Institute of Technology, Wright-Patterson AFB, Ohio, Attn: MCLI-ITRIDL	1
BSD, Norton AFB, California	1
Director, USAF Project RAND, Via: U.S. Air Force Liaison Office, The Rand Corporation, 1700 Main Street, Santa Monica, California Attn: Dr. H. L. Brode	1
Director of Civil Engineering, Hq USAF, Washington 25, D. C. Attn: AFOCE	1

OTHERS	Copies
Director of Defense Research & Engineering, Washington 25, D. C. Attn: Tech Library	1
U.S. Documents Officer, Office of the United States National Military Representative-SHAPE, APO 55, New York, N. Y.	1
Commander-in-Chief, Pacific, Fleet Post Office, San Francisco, California	1
Director, Weapons Systems Evaluation Group, OSD, Room 1E880, The Pentagon, Washington 25, D. C.	1
Commandant, Armed Forces Staff College, Norfolk 11, Virginia Attn: Library	1
Commander, Field Command, DASA, Sandia Base, Albuquerque, New Mexico	16
Commander, Field Command, DASA, Sandia Base, Albuquerque, New Mexico, Attn: FCWT Attn: FCTG	1 1
Chief, Defense Atomic Support Agency, Washington 25, D. C.	5
Commandant, Army War College, Carlisle Barracks, Pennsylvania Attn: Library	1
Commandant, National War College, Washington 25, D. C. Attn: Class Rec. Library	1
Commandant, The Industrial College of the Armed Forces, Ft McNair, Washington 25, D. C.	1
Officer-in-Charge, U.S. Naval School, Civil Engineering Corps Officers, U.S. Naval Construction Battalion, Port Hueneme, California	1
Los Alamos Scientific Laboratory, P. O. Box 1663, Los Alamos, New Mexico, Attn: Dr. A. C. Graves, Dr. W. C. Davis	2
Administrator, National Aeronautics & Space Administration, 1512 H Street, N.W., Washington 25, D. C.	1
Langley Research Center, NASA, Langley Field, Hampton, Virginia Attn: Mr. Philip Donely	1
Chief, Classified Technical Library, Technical Information Service, U.S. Atomic Energy Commission, Washington 25, D. C. Attn: Mrs. Jean O'Leary (for Dr. Paul C. Fine)	1

OTHERS CONT'D	Copies
Chief, Classified Technical Library, Technical Information Service U.S. Atomic Energy Commission, Washington 25, D. C. Attn: Mrs. Jean O'Leary	1
Forestal Research Center Library, Aeronautical Sciences Bldg., Princeton University, Princeton, N. J., Attn: Librarian (for Dr. Walker Bleakney)	1
Manager, Albuquerque Operations Office, U.S. Atomic Energy Commission, P. O. Box 5400, Albuquerque, New Mexico	1
Sandia Corporation, Sandia Base, Albuquerque, New Mexico Attn: Dr. M. L. Merritt, W. B. Benedick, W. Roberts, J. W. Reed, Dr. C. Broyles	5
United Research Services, 1811 Trousdale Drive, Burlingame, California, Attn: Mr. Kenneth Kaplan	1
Department of Physics, Stanford Research Institute, Menlo Park, California, Attn: Mr. Fred M. Sauer	1
Southwest Research Institute, P. O. Box 28281, San Antonio 6, Texas, Attn: Dr. Robert C. DeHart	1
Space Technology Laboratories, Inc., 5500 West El Segunda Blvd., Los Angeles 45, California, Attn: Dr. Leon	1
Kaman Nuclear, Colorado Springs, Colorado Attn: Dr. Frank Shelton	1
E. O. Lawrence Radiation Laboratory, University of California, P. O. Box 808, Livermore, California, Attn: Tech Information Div.	1
National Aeronautics and Space Administration, Manned Spacecraft Center, Space Technology Division, Box 1537, Houston, Texas Attn: Mr. R. F. Fletcher	1
Armour Research Foundation, 10 West 35th Street, Chicago 16, Ill. Attn: Dr. T. H. Schiffman	1
Institute for the Study of Rate Processes, University of Utah, Salt Lake City, Utah, Attn: Dr. M. A. Cook	1
Denver Research Institute, Mechanics Division, University of Denver, Denver 10, Colorado, Attn: Mr. Rodney F. Recht	2
Director, New Mexico Institute of Mining Technology, Socorro, New Mexico, Attn: Dr. M. Kempton	1

OTHERS CONT'D	Copies
Director, Applied Physics Laboratory, Johns Hopkins University, 8621 Georgia Avenue, Silver Spring, Maryland, Attn: Tech Library	1
Director, U.S. Bureau of Mines, Division of Explosive Technology, 4800 Forbes Street, Pittsburgh 13, Pennsylvania Attn: Dr. Robert W. Van Dolah	1
Chairman, Armed Services Explosives Safety Board, Bldg T-7, Gravelly Point, Washington 25, D. C., Attn: Mr. R. G. Perkins	1
Science Communication, Inc., 1079 Wisconsin Avenue, N. W., Washington 7, D. C., Attn: Mr. D. O. Myatt	1
Edgerton, Germeshausen, and Grier, Inc., 160 Brookline Avenue, Boston 15, Mass., Attn: D. F. Hansen	1
Office of Technical Services, Department of Commerce, Washington 25, D. C.	100
Commander, DDC , Arlington Hall Station, Arlington 12, Virginia, Attn: TIPDR	10

CATALOGING INFORMATION FOR LIBRARY USE

BIBLIOGRAPHIC INFORMATION

	DESCRIPTORS	CODES		DESCRIPTORS	CODES
SOURCE	NOL technical report	NOLTR	SECURITY CLASSIFICATION AND CODE COUNT	Unclassified - 28	UØ28
REPORT NUMBER	62-182	62Ø182	CIRCULATION LIMITATION		
REPORT DATE	9 November 1962	1162	CIRCULATION LIMITATION OR BIBLIOGRAPHIC	Part I	PRTB1
			BIBLIOGRAPHIC (SUPPL., VOL., ETC.)		

SUBJECT ANALYSIS OF REPORT

DESCRIPTORS	CODES	DESCRIPTORS	CODES	DESCRIPTORS	CODES
Origin	ORGI	Ambient	ENVI	Pressures	PRES
Shockwaves	SHAV	Conditions	CNDI	Cast	CAST
Explosions	EXPS	Phenomena	PHEO	Detonation (effects)	DETOE
Air	ATMO	Beckman-Whitley	BECW	Shock (effects)	SHOCE
Spherical	SPHE	Camera	CAME		
Condensed	CODO	Shape	SHAP		
Shock	SHOC	Detonation	DETO		
Photographic	PHOT	Transmission	TRAS		
Observations	OBSR	Front	FRON		
Pentolite	PENI	Velocity	VELC		
Explosive	EXPL	Experimental	EXPE		
Hemispheres	HEMI	Charges	CHAR		

PRNC-NOL-5070/28 (5-62)

Naval Ordnance Laboratory, White Oak, Md.
(NOL technical report 62-132)
ON THE ORIGIN OF SHOCKWAVES FROM SPHERICAL CONDENSED EXPLOSIONS IN AIR. PART I. RESULTS OF PHOTOGRAPHIC OBSERVATIONS OF PENTOLITE HEMISPHERES AT AMBIENT CONDITIONS (U), by L. Rudlin. 9 Nov. 1962. 25p. illus., tables. (DASA-1360) NOL task 181.

UNCLASSIFIED

The phenomena occurring during the explosion of pentolite hemispheres are observed using the Beckman-Whitley camera operated at 0.5μ second intervals. The observations indicate that the airshock formed outside the explosive results from the transmission of the detonation shockfront into the air. The airshock velocity appears to remain constant, at the detonation-velocity value of 7730 m/sec, for several microseconds before decaying.

1. Explosions - Shockwaves
2. Explosions - Photography
3. Pentolite - Blast effects

I. Title
II. Title: Results of photographic observations of pentolite hemispheres at ambient conditions
III. Rudlin, Leonard
IV. Series
V. Project

Naval Ordnance Laboratory, White Oak, Md.
(NOL technical report 62-132)
ON THE ORIGIN OF SHOCKWAVES FROM SPHERICAL CONDENSED EXPLOSIONS IN AIR. PART I. RESULTS OF PHOTOGRAPHIC OBSERVATIONS OF PENTOLITE HEMISPHERES AT AMBIENT CONDITIONS (U), by L. Rudlin. 9 Nov. 1962. 25p. illus., tables. (DASA-1360) NOL task 181.

UNCLASSIFIED

The phenomena occurring during the explosion of pentolite hemispheres are observed using the Beckman-Whitley camera operated at 0.5μ second intervals. The observations indicate that the airshock formed outside the explosive results from the transmission of the detonation shockfront into the air. The airshock velocity appears to remain constant, at the detonation-velocity value of 7730 m/sec, for several microseconds before decaying.

1. Explosions - Shockwaves
2. Explosions - Photography
3. Pentolite - Blast effects

I. Title
II. Title: Results of photographic observations of pentolite hemispheres at ambient conditions
III. Rudlin, Leonard
IV. Series
V. Project

Naval Ordnance Laboratory, White Oak, Md.
(NOL technical report 62-132)
ON THE ORIGIN OF SHOCKWAVES FROM SPHERICAL CONDENSED EXPLOSIONS IN AIR. PART I. RESULTS OF PHOTOGRAPHIC OBSERVATIONS OF PENTOLITE HEMISPHERES AT AMBIENT CONDITIONS (U), by L. Rudlin. 9 Nov. 1962. 25p. illus., tables. (DASA-1360) NOL task 181.

UNCLASSIFIED

The phenomena occurring during the explosion of pentolite hemispheres are observed using the Beckman-Whitley camera operated at 0.5μ second intervals. The observations indicate that the airshock formed outside the explosive results from the transmission of the detonation shockfront into the air. The airshock velocity appears to remain constant, at the detonation-velocity value of 7730 m/sec, for several microseconds before decaying.

1. Explosions - Shockwaves
2. Explosions - Photography
3. Pentolite - Blast effects

I. Title
II. Title: Results of photographic observations of pentolite hemispheres at ambient conditions
III. Rudlin, Leonard
IV. Series
V. Project

Naval Ordnance Laboratory, White Oak, Md.
(NOL technical report 62-132)
ON THE ORIGIN OF SHOCKWAVES FROM SPHERICAL CONDENSED EXPLOSIONS IN AIR. PART I. RESULTS OF PHOTOGRAPHIC OBSERVATIONS OF PENTOLITE HEMISPHERES AT AMBIENT CONDITIONS (U), by L. Rudlin. 9 Nov. 1962. 25p. illus., tables. (DASA-1360) NOL task 181.

UNCLASSIFIED

The phenomena occurring during the explosion of pentolite hemispheres are observed using the Beckman-Whitley camera operated at 0.5μ second intervals. The observations indicate that the airshock formed outside the explosive results from the transmission of the detonation shockfront into the air. The airshock velocity appears to remain constant, at the detonation-velocity value of 7730 m/sec, for several microseconds before decaying.

1. Explosions - Shockwaves
2. Explosions - Photography
3. Pentolite - Blast effects

I. Title
II. Title: Results of photographic observations of pentolite hemispheres at ambient conditions
III. Rudlin, Leonard
IV. Series
V. Project

Naval Ordnance Laboratory, White Oak, Md.
(NOL technical report 62-132)
ON THE ORIGIN OF SHOCKWAVES FROM SPHERICAL CONDENSED EXPLOSIONS IN AIR. PART I. RESULTS OF PHOTOGRAPHIC OBSERVATIONS OF PENTOLITE HEMISPHERES AT AMBIENT CONDITIONS (U), by L. Rudlin. 9 Nov. 1962. 25p. illus., tables. (DASA-1360) NOL task 181.

UNCLASSIFIED

The phenomena occurring during the explosion of pentolite hemispheres are observed using the Beckman-Whitley camera operated at 0.5 μ second intervals. The observations indicate that the airshock formed outside the explosive results from the transmission of the detonation shockfront into the air. The airshock velocity appears to remain constant, at the detonation-velocity value of 7730 m/sec, for several microseconds before decaying.

1. Explosions - Shockwaves
2. Explosions - Photography
3. Pentolite - Blast effects
I. Title
II. Title: Results of photographic observations of pentolite hemispheres at ambient conditions
III. Rudlin, Leonard
IV. Series
V. Project

Naval Ordnance Laboratory, White Oak, Md.
(NOL technical report 62-132)
ON THE ORIGIN OF SHOCKWAVES FROM SPHERICAL CONDENSED EXPLOSIONS IN AIR. PART I. RESULTS OF PHOTOGRAPHIC OBSERVATIONS OF PENTOLITE HEMISPHERES AT AMBIENT CONDITIONS (U), by L. Rudlin. 9 Nov. 1962. 25p. illus., tables. (DASA-1360) NOL task 181.

UNCLASSIFIED

The phenomena occurring during the explosion of pentolite hemispheres are observed using the Beckman-Whitley camera operated at 0.5 μ second intervals. The observations indicate that the airshock formed outside the explosive results from the transmission of the detonation shockfront into the air. The airshock velocity appears to remain constant, at the detonation-velocity value of 7730 m/sec, for several microseconds before decaying.

1. Explosions - Shockwaves
2. Explosions - Photography
3. Pentolite - Blast effects
I. Title
II. Title: Results of photographic observations of pentolite hemispheres at ambient conditions
III. Rudlin, Leonard
IV. Series
V. Project

Naval Ordnance Laboratory, White Oak, Md.
(NOL technical report 62-132)
ON THE ORIGIN OF SHOCKWAVES FROM SPHERICAL CONDENSED EXPLOSIONS IN AIR. PART I. RESULTS OF PHOTOGRAPHIC OBSERVATIONS OF PENTOLITE HEMISPHERES AT AMBIENT CONDITIONS (U), by L. Rudlin. 9 Nov. 1962. 25p. illus., tables. (DASA-1360) NOL task 181.

UNCLASSIFIED

The phenomena occurring during the explosion of pentolite hemispheres are observed using the Beckman-Whitley camera operated at 0.5 μ second intervals. The observations indicate that the airshock formed outside the explosive results from the transmission of the detonation shockfront into the air. The airshock velocity appears to remain constant, at the detonation-velocity value of 7730 m/sec, for several microseconds before decaying.

1. Explosions - Shockwaves
2. Explosions - Photography
3. Pentolite - Blast effects
I. Title
II. Title: Results of photographic observations of pentolite hemispheres at ambient conditions
III. Rudlin, Leonard
IV. Series
V. Project

Naval Ordnance Laboratory, White Oak, Md.
(NOL technical report 62-132)
ON THE ORIGIN OF SHOCKWAVES FROM SPHERICAL CONDENSED EXPLOSIONS IN AIR. PART I. RESULTS OF PHOTOGRAPHIC OBSERVATIONS OF PENTOLITE HEMISPHERES AT AMBIENT CONDITIONS (U), by L. Rudlin. 9 Nov. 1962. 25p. illus., tables. (DASA-1360) NOL task 181.

UNCLASSIFIED

The phenomena occurring during the explosion of pentolite hemispheres are observed using the Beckman-Whitley camera operated at 0.5 μ second intervals. The observations indicate that the airshock formed outside the explosive results from the transmission of the detonation shockfront into the air. The airshock velocity appears to remain constant, at the detonation-velocity value of 7730 m/sec, for several microseconds before decaying.

1. Explosions - Shockwaves
2. Explosions - Photography
3. Pentolite - Blast effects
I. Title
II. Title: Results of photographic observations of pentolite hemispheres at ambient conditions
III. Rudlin, Leonard
IV. Series
V. Project

UNCLASSIFIED